ARTICLE IN PRESS

Communications Biology

https://doi.org/10.1038/s42003-026-09530-0

Article in Press

Differentially expressed miRNAs in the temporal cortex of Alzheimer's disease patients and their association to tau pathology

Received: 15 April 2025

Accepted: 5 January 2026

Cite this article as: Nagaraj, S., Quintanilla-Sánchez, C., Ando, K. *et al.* Differentially expressed miRNAs in the temporal cortex of Alzheimer's disease patients and their association to tau pathology. *Commun Biol* (2026). https://doi.org/10.1038/s42003-026-09530-0

Siranjeevi Nagaraj, Carolina Quintanilla-Sánchez, Kunie Ando, Lidia Lopez-Gutierrez, Yannick Gansemans, Emilie Doeraene, Andreea-Claudia Kosa, Emmanuel Aydin, Filip Van Nieuwerburgh, Jean-Pierre Brion & Karelle Leroy

We are providing an unedited version of this manuscript to give early access to its findings. Before final publication, the manuscript will undergo further editing. Please note there may be errors present which affect the content, and all legal disclaimers apply.

If this paper is publishing under a Transparent Peer Review model then Peer Review reports will publish with the final article.

ARTICLE IN PRESS

© The Author(s) 2026. **Open Access** This article is licensed under a Creative Commons Attribution-NonCommercial-NoDerivatives 4.0 International License, which permits any non-commercial use, sharing, distribution and reproduction in any medium or format, as long as you give appropriate credit to the original author(s) and the source, provide a link to the Creative Commons licence, and indicate if you modified the licensed material. You do not have permission under this licence to share adapted material derived from this article or parts of it. The images or other third party material in this article are included in the article's Creative Commons licence, unless indicated otherwise in a credit line to the material. If material is not included in the article's Creative Commons licence and your intended use is not permitted by statutory regulation or exceeds the permitted use, you will need to obtain permission directly from the copyright holder. To view a copy of this licence, visit http://creativecommons.org/licenses/by-nc-nd/4.0/.

ARTICLE IN PRESS

Differentially expressed miRNAs in the temporal cortex of Alzheimer's disease patients and their association to tau pathology.

Siranjeevi Nagaraj[1 #*], Carolina Quintanilla Sanchez[1#], Kunie Ando[1], Lidia Lopez Gutierrez[1], Yannick Gansemans[2], Emilie Doeraene[1], Andreea-Claudia Kosa[1], Emmanuel Aydin[1], Filip Van Nieuwerburgh[2], Jean-Pierre Brion[1] and Karelle Leroy[1*]

[1] Alzheimer and Other Tauopathies Research Group, ULB Neuroscience Institute (UNI), ULB Center for Diabetes Research (UCDR), Faculty of Medicine, Université Libre de Bruxelles, Brussels, Belgium.
[2] Laboratory of Pharmaceutical Biotechnology, Faculty of Pharmaceutical Sciences, Ghent University, Ghent, Belgium.

*Correspondence: Karelle.Leroy@ulb.be; siranjeevi.nagaraj@ulb.be.

# Authors contributed equally to this work

Abstract

Alzheimer's disease (AD) is a major contributor to dementia in the elderly, characterized by progressive impairments in memory and behaviour. AD is marked by pathological hallmarks: amyloid plaques and neurofibrillary tangles (NFTs). Despite extensive efforts to understand these hallmarks, there is still a lack of efficient therapeutic approaches due to limited knowledge of the fundamental cellular mechanisms underlying the disease. One potential avenue of research involves the investigation of the roles of non-coding RNAs, particularly microRNAs (miRNAs), which bind to the 3' UTRs of target mRNAs to suppress expression. In our study, we analyse the temporal superior T1 isocortex of control and AD patients, identifying differentially expressed miRNAs using next-generation sequencing (NGS). To validate these findings, we utilize an additional technique, RT-qPCR. Our study confirms the previous findings on the dysregulation of miR-129-5p, miR-132-3p, and miR-146b-5p, while also provides insights into the dysregulation of miR-151a-5p and miR-1-3p. Importantly, the expression levels of miR-129-5p, miR-146b-5p, miR-132-3p, and miR-151a-5p are significantly correlated with the neuropathological Braak stages and with biochemically quantified tau phosphorylation levels in brain homogenates. Additionally, we find that miR-146b-5p and miR-151a-5p significantly modulate tau seeding in tau biosensor cell model, highlighting their potential roles in tau pathology.

ARTICLE IN PRESS

Introduction

Alzheimer's disease (AD) is the most common cause of dementia in the elderly population, resulting in a significant socioeconomic burden[1]. The neuropathological lesions of AD include extracellular amyloid plaques, composed of amyloid β (Aβ) peptides derived from the cleavage of amyloid precursor protein (APP), and intracellular neurofibrillary tangles (NFTs), composed of hyperphosphorylated tau, forming paired helical filaments (PHF)[2-6]. Due to the disease's multifaceted complexity, effective disease-modifying therapies remain unavailable[7,8]. Consequently, there is a critical need to identify neuroprotective strategies by investigating the molecular pathways implicated in AD pathology.

Increasing evidence suggests significant roles of non-coding RNAs, including microRNAs (miRNAs; <25 nucleotides), long non-coding RNAs (lncRNAs; >200 nucleotides), circular RNAs, transfer RNA-derived small RNAs (tsRNAs) and piwi-interacting RNA (piRNAs) in physiological and pathological conditions[9-11]. Among these, miRNAs represent a class of short non-coding RNA molecules that play a crucial role in the epigenetic regulation of gene expression at the post-transcriptional level. Through specific partial sequence base pairing, miRNAs bind to the 3' untranslated region (3' UTR) of their target transcripts and

ARTICLE IN PRESS

reduce their expression by either mRNA degradation or translational inhibition[12-14]. A growing body of literature shows that miRNAs are dysregulated in the brain, cerebrospinal fluid (CSF), and blood of AD patients[10,15]. Importantly, some studies have linked the miRNAs dysregulation in AD brains to tau and amyloid pathways[16-19].

Currently, the number of studies exploring differential miRNAs in AD post-mortem brain samples is limited, and additional research is essential to identify their roles in AD pathology and validate dysregulated miRNAs as a basis for hypothesis-driven experimentation. For instance, a meta-analysis of 11 studies using all the regions of post-mortem brain samples in a combined cohort of 122 subjects (58 control and 64 AD) demonstrated that miR-125b-5p is strongly upregulated in AD[15]. However, an independent study using a larger cohort of 190 subjects (91 control and 99 AD) revealed no significant changes in miR-125b-5p expression in the superior temporal gyrus of AD patients[20]. These discrepancies underline the need for further validation in additional AD post-mortem cohort, which should be invaluable not only for identifying novel dysregulated miRNAs, but also for confirming or revising previously identified miRNAs to strengthen their relevance to AD pathology.

In our study, we employed next-generation sequencing (NGS) to compare the differential expression of miRNAs in the temporal superior T1 isocortex of control and AD patients. Additionally, we validated the dysregulation of selected miRNAs using RT-qPCR in a cohort of 36 subjects (13 control and 23 AD). We attempted to shed light on the correlation between miRNA expression and tau pathology progression, based on Braak staging and biochemical protein quantification from brain homogenates. Additionally, we employed HEK fluorescence resonance energy transfer (FRET) biosensor cell lines to assess the impact of specific miRNAs on tau seeding activity of pathological tau present in human AD fractions. This study provides a better understanding of miRNA dysregulation in AD and its potential implications in tau pathology progression and therapeutic intervention.

Methods

Human samples

Samples from the temporal superior T1 isocortex were obtained from control subjects (n=13, Braak stages 0 to III) and AD (n=23, Braak stages V-VI). Control and AD subjects were diagnosed according to the National Institute of Aging and Reagan Institute Criteria[21] and scored by neuropathological staging for tau pathology[22]. Some of the subjects were also scored for Thal staging **(Table 1)**[23]. Apolipoprotein E (APOE) genotype was identified for the subjects with an informed consent for genetic study using PCR amplification for genomic DNA and sequencing. Sarkosyl-insoluble fractions were obtained from the frontal cortex of post-mortem brain samples. We used brain samples from Neuro-CEB (France) and ULB LHNN (Belgium) brain banks as shown in the **Table 1.** For Neuro-CEB, procedure of the brain bank was approved by the ethical committee "Comité de Protection des Personnes Paris Ile de France VI" and for ULB LHNN brain bank (BB190052), approval was obtained from the ethical committee of the medical school of the Université Libre de Bruxelles (ULB), Belgium (P2009/015). Autopsies and biochemical analyses were carried out after written informed consent was obtained from family members. All ethical regulations relevant to human research participants were followed.

Total RNA extraction and quality analysis

ARTICLE IN PRESS

Total RNA was extracted from approximately 100 mg of the temporal superior T1 isocortex brain regions (13 control and 23 AD) using mirVana PARIS RNA and Native Protein Purification Kit (Thermo Fisher Scientific) following the manufacturer's protocol. Extracted RNA samples were treated with DNase using TURBO DNA-free kit (Thermo Fisher Scientific). Quality of RNA samples was checked using DNF-472 RNA (15 nt) HS RNA Kit on Fragment Analyzer (Agilent Technologies) and quantification was done using Quant-it Ribogreen assay (Thermo Fisher Scientific). Only 19 samples (9 control and 10 AD) with RIN value ≥ 3.5 were proceeded to the miRNA library preparation and sequencing **(Table 1 and Fig. 1d).**

miRNA sequencing and data analysis

For each sample, a sequencing library was constructed with 200 ng input RNA using the QIAseq miRNA Library Kit (Qiagen). This kit appends a 19 nt spacer and 12 nt unique molecular identifier (UMI) at the 3'-end of the original small RNA in the forward read (read 1), enabling PCR duplicate identification and amplification bias correction. Libraries were amplified using 15 PCR cycles, size-selected on an 8% native PAGE gel (Invitrogen) and purified. Library quality was assessed with the DNF-474 HS NGS Fragment (1-6000 bp) Kit on a Fragment Analyzer (Agilent Technologies) and quantified using the 'Sequencing Library qPCR Quantification Guide' from Illumina. Equimolar-pooled libraries were spiked with 15% PhiX as an internal control and sequenced as single-read 76 on a NextSeq 500 platform (Illumina).

Reads lacking a detectable spacer and UMI were discarded using UMI-tools (v1.1.2)[24]. The remaining reads were assessed for quality and length using FastQC (v0.12.1) and screened for potential contaminants against a panel of common laboratory organism genomes using FastQ Screen (v0.15.3)[25]. PCR duplicates, defined as reads with identical UMI and sequence, were collapsed to retain only one representative per group. Known miRNA identification, novel miRNA prediction, and expression quantification were performed using the mirPRo pipeline (v1.1.4)[26] with the latest miRBase (v22.1) annotations and the human genome (GRCh38, ENSEMBL release 111). The miRBase database contains 2656 mature human miRNA sequences[27]. For novel miRNA prediction, reference data from all mammalian species in miRBase were used. Differential gene expression analysis was done in R (v4.3.3) using the edgeR (4.0.16) package[28]. Briefly, feature counts were TMM-normalized and dispersions were estimated. For pairwise comparison of gene expressions between conditions, we used the quasi-likelihood model and F-test for a more reliable error rate. Correction of the p values for repeated testing was done with the Benjamini-Hochberg method.

RT-qPCR analysis

Briefly, 30 ng of RNA isolated from post-mortem temporal superior T1 isocortex samples was used for reverse transcription to obtain the cDNA using the miRCURY LNA RT Kit (339340, Qiagen). Quantitative PCR was performed according to manufacturer's protocol using cDNA template, miRCURY SYBR green master mix (339346, Qiagen) and miRCURY LNA miRNA assays (339306, Qiagen) **(Supplementary Table 4)** in CFX96 Touch Real time PCR (Biorad). Cycle thresholds (Ct) were obtained for target miRNAs (miR-129-5p, miR-146b-5p, miR-151a-5p, miR-1-3p, miR-132-3p, miR-18a-5p, miR-132-5p, miR-133a-3p, miR-151b, miR-3065-3p, miR-129-1-3p) and normalizers. We used both small RNA U6 and two miRNAs (miR-16-5p and miR-30b-5p) identified via sequencing experiment as non-differentially expressed miRNAs as normalizer for relative quantification using $2(-\Delta\Delta C(T))$ method[29].

Preparation of RIPA-soluble fractions

ARTICLE IN PRESS

RIPA-soluble fractions were obtained as previously described[30]. Briefly, 200 mg of frozen temporal superior T1 isocortex was homogenized in 10 volumes of ice-cold RIPA buffer (containing 50 mM Tris–HCl pH 7.4, 50 mM NaCl, 1% NP-40, 0.25% sodium deoxycholate) with 5 mM EDTA, 1 mM EGTA, complete protease inhibitor cocktail (Merck), 1 mM PMSF (Sigma), and phosphatase inhibitor cocktail 2 (Sigma). The homogenate was rotated for 1 hour at 4 °C, centrifuged at 20,000 g for 20 min at 4 °C, and the resulting supernatant was used as the RIPA-soluble fractions to quantify phosphorylated tau (pTau).

Preparation of sarkosyl-insoluble fractions

Sarkosyl-insoluble fractions were obtained as previously described [30,31]. Briefly, 0.5 g of frontal cortex from post-mortem brain samples were homogenized in 10 volumes of ice-cold PHF-extraction buffer (10 mM Tris–HCl pH 7.4, 0.8 M NaCl, 1 mM EDTA, and 10% sucrose) and subsequently centrifuged at 15,000 g for 20 min at 4 °C. Supernatant was obtained and N-lauroylsarcosine sodium salt (Sigma) was added to have final concentration of 1% (w/v). Following overnight incubation at 4 °C with gentle agitation, ultracentrifugation was carried out at 180,000 g for 30 min at 4 °C. Sarkosyl-insoluble pellet containing PHF was gently rinsed with PBS and resuspended by vortexing and pipetting in PBS. Sarkosyl-insoluble fraction was sonicated on ice by a probe-sonicator (amplitude 20, 10 pulses of one second with one second of interval). After Bradford protein quantification (BioRad), sarkosyl-insoluble fractions were aliquoted and kept at −20 °C until further use. Sarkosyl-insoluble fractions were analysed by western blotting (WB) and transmission electron microscopy (TEM) as previously described[32,33]. These sarkosyl-insoluble fractions were used to induce tau seeding detected by fluorescence resonance energy transfer (FRET) assays in HEK tau biosensor cells.

Western blotting

A total of 100 µg of RIPA-soluble fractions and 5 µg of sarkosyl-insoluble fractions diluted in Laemmli buffer containing 2-mercaptoethanol, denatured for 10 min at 100 °C, were loaded in each well and separated by 10% Tris–glycine SDS-PAGE gels. After electrophoretic separations, proteins were transferred to nitrocellulose membranes using a transfer unit (BioRad). Membranes were blocked with 10% semifat dry milk for 2 h and incubated overnight at 4 °C with primary antibodies: PHF1 (1:1000, from Dr. Peter Davies)[34], Total tau (1:2000, DAKO A0024) and actin (1:1000, Sigma A2066). Next day, secondary antibodies (1:5000, anti-rabbit CST#7074 or 1:5000, anti-mouse CST#7076) conjugated to horseradish peroxidase was used to target the primary antibodies. Detection of the immunoreaction was performed with a SuperSignal West Pico PLUS enhanced chemiluminescence substrate kit (Thermo Fisher Scientific) using a Fusion SOLO 4S system (Vilber-Lourmat).

Tau seeding assay

Tau RD P301S FRET biosensor HEK293T cells (referred to as HEK tau biosensor cells) were purchased from ATCC (CRL-3275) and were grown in Dulbecco's Modified Eagle Medium (DMEM) medium supplemented with 10% foetal bovine serum (FBS), 100 IU penicillin and 100 µg of streptomycin and 2 mM L-glutamine. Cells were cultured at 37 °C in a humidified atmosphere of 5% CO_2. HEK tau biosensor cells stably express tau repeat domain (RD) sequence with P301S mutation conjugated to either cyan fluorescent protein (CFP) or yellow fluorescent protein (YFP)[35]. Under untreated conditions or with the addition of sarkosyl-insoluble fractions from a healthy control, there was no FRET signal, which was considered as baseline. However, upon adding sarkosyl-insoluble fractions from AD patients, it exhibited FRET signals as previously described[36]. HEK tau biosensor cells were seeded at the density of $4x10^4$ cells/well in 12 well plate. On the second day miRNA mimics (Horizon Discovery: C-300538-05, C-300754-03, C-301086-01, C-

ARTICLE IN PRESS

300585-05, C-300599-06) or miRNA inhibitors (Horizon Discovery: IH-300538-07, IH-300754-05, IH-301086-02, IH-300585-06, IH-300599-05) at 20 nM concentration were transfected and on the third day 1 µg sarkosyl-insoluble fractions from AD patient were added. On the fifth day, cells were collected in 2% FBS in 1x PBS buffer. Cellular FRET signals were measured as integrated FRET density by fluorescence-activated cell sorting (FACS) in BD LSR Fortessa X-20 Cell Analyzer. Briefly, to measure CFP and FRET, the cells were excited with a 405 nm laser, and emission was detected through 450/50 nm and 525/50 nm filters, respectively. YFP excitation was performed with a 488 nm laser, and emission was detected using a 530/30 nm filter[35,36]. For comparative analysis between AD PHF + miRNA mimic and AD PHF + miRNA inhibitor, the integrated FRET density of AD PHF alone was used as a normalizer.

Target and Pathway enrichment analysis

miRNet web-based tool was used to identify the miRNA-target network and Kyoto Encyclopedia of Genes and Genomes (KEGG) enrichment analysis for predicted targets of downregulated and upregulated miRNAs[37,38].

Statistics and reproducibility

Welch Two Sample t-test was used for comparisons of age, post-mortem delay (PMD), RIN values between the control (n=9) and AD patients (n=10). Fisher's Exact Test was used for the comparison of sex distributions (control (n=9; 8 males and 1 female) and AD patients (n=10; 3 males and 7 females)). Pairwise comparison was used to identify differential expression of miRNAs with criteria p value <0.003 and FDR/padj < 0.1 in the cohort (control, n=9; AD, n=10). For RT-qPCR ((control, n=9; AD, n=10) or (control, n=13; AD, n=23)) and FACS experiments (n=3), either Welch Two Sample t-test or one-way ANOVA with post–hoc Tukey HSD (Honestly significant difference) test was performed as in the figure description. For correlation analysis, Spearman correlation ((control, n=9; AD, n=10) or (control, n=13; AD, n=23)) was used. All statistics were performed using R (https://www.R-project.org/) and p value < 0.05 was considered statistically significant. For human post-mortem brain samples, the sample size (n) used is mentioned in the figure description and replicates were defined at the subject level (individual person). For in vitro HEK biosensor cells, n=3 was used. For KEGG enrichment analysis, statistically significant annotations with FDR<0.05 were considered and R was used for visualization.

Data availability

The miRNA sequencing datasets are available in Gene Expression Omnibus (GEO) through accession number: GSE309036. Numerical source data for graphs and charts can be found in Supplementary data 1. All other data are available from the corresponding author on reasonable request.

Results

Cohort demographics and RNA quality analysis

In our cohort, we grouped subjects with Braak stages up to III as control and subjects with Braak stages V-VI as AD. In our study, temporal superior T1 isocortex from 36 subjects (control, n=13; AD, n=23) were processed for RNA extraction and quality analysis **(Table 1)**. For these 36 subjects, we obtained variable RNA quality indicated by RIN with minimum RIN=2.3 and maximum RIN=7.6 **(Fig. 1a-b and Table 1)**. Such variable RNA quality is reported in several post-mortem brain samples in both control and AD[20,39]. **Fig. 1c** illustrates the minimum and maximum RIN values obtained in several reports exploring differential

ARTICLE IN PRESS

miRNAs expression in post-mortem brain samples in AD[20,39-44]. In our cohort, correlation analysis suggested that there is no association between the RIN and PMD **(Supplementary Fig. 1a-c)**. Based on the RIN cut-off of ≥ 3.5, we selected 19 subjects (control, n=9; AD, n=10) **(Fig. 1b and Table 1)**. We have chosen this cut-off where we can observe the ribosomal RNAs in the digital gel of the Agilent analyzer **(Fig. 1a)**, suggesting that the samples are not completely degraded. Also, a recent study showed that the average RIN for n=190 samples used was around 3.6[20]. This implies that the minimum quality of the RNA samples used in this study is comparable to the average RIN quality used in similar studies. Interestingly, in these selected 19 subjects we found a trend for negative correlation between the RIN and PMD (R=-0.4 and p=0.094) **(Fig. 1b)** but not in complete group of 36 subjects (R=-0.18 and p=0.31) **(Supplementary Fig. 1a)**. All subsequent analysis were done for only these 19 subjects, unless explicitly mentioned. The average age at death was 72.11 ± 2.61 years for the control subjects (n=9) and 76.6 ± 3.81 years for AD subjects (n=10) (mean ± standard error of the mean) (t-test, p=0.35). Similarly, the average PMD was 19.06 ± 4.39 hours for control subjects and 18.80 ± 3.14 hours for AD subjects (mean ± standard error of the mean) (t-test, p=0.96). The average RIN was 4.96 ± 0.47 for control subjects and 5.43 ± 0.50 for AD subjects (mean ± standard error of the mean) (t-test, p=0.49). These comparisons showed no significant differences in age, PMD, or RIN values between the control and AD groups. However, a significant difference in sex distribution was observed between the control group (n=9; 8 males and 1 female) and the AD group (n=10; 3 males and 7 females) (Fisher's Exact Test, p=0.019) **(Table 1).**

Differential miRNA expression in temporal cortex region in AD patients- Screening by NGS

We investigated differential expression of miRNAs in the temporal superior T1 isocortex, comparing 9 controls to 10 AD individuals. Among the 449 miRNAs that were detected by NGS, 12.7 percent (57 of the 449 miRNAs) of them had unadjusted p value <0.05. However, after Benjamini-Hochberg (BH) procedure of false discovery rate (FDR) adjustment, none of them had adjusted p value (padj) <0.05. 13 miRNAs were considered differentially expressed miRNAs with the criteria of p value <0.003, FDR or padj < 0.1 and |log2 fold change|>=0.45 **(Fig. 1d and Supplementary Table 1)**. At this threshold (FDR < 0.1), up to 10% of the identified miRNAs are expected to be false positives. Thus, on average, around 1 to 2 of the 13 miRNAs may be false positives. Volcano plot shows 5 upregulated miRNAs shown in red (miR-18a-5p, miR-151a-5p, novel-miR-122, miR-151b, and miR-3065-3p) and 8 downregulated miRNAs shown in blue (miR-129-5p, miR-146b-5p, miR-132-5p, miR-133a-3p, miR-1-3p, novel-miR-71, miR-132-3p, and miR-129-1-3p) in AD compared to the control **(Fig. 1e)**. Among these 13 miRNAs, based on the normalized NGS counting 5 were high abundance miRNAs (average normalized counts >400): miR-129-5p, miR-146b-5p, miR-151a-5p, miR-1-3p, and miR-132-3p and 8 were low abundance miRNAs (average normalized counts <400): miR-18a-5p, miR-132-5p, miR-133a-3p, miR-151b, miR-3065-3p, miR-129-1-3p, novel-miR-71, and novel-miR-122. Box plot in **Fig. 2** shows differential expression of these 13 miRNAs among the control and AD. Notably, RIN, PMD, and age showed no significant correlation with miRNA expression **(Fig. 3a and Supplementary Fig. 1d)**. Stratification by brain bank (Neuro-CEB vs. ULB LHNN) or group (control vs. AD) revealed no major associations **(Supplementary Fig. 1e–f)**, except for a correlation between PMD and miR-146b-5p in control when stratified by group. When we analysed 5 differentially expressed miRNAs of high abundance in AD versus control, all the downregulated miRNAs miR-129-5p, miR-146b-5p, miR-1-3p, and miR-132-3p were negatively correlated with upregulated miR-151a-5p **(Fig. 3a-b)**. Within these 5 highly abundant miRNAs, the downregulated miRNAs (miR-129-5p, miR-146b-5p, miR-1-3p, and miR-132-3p) in AD showed positive correlations with each other, although only some were statistically significant (miR-129-5p vs. miR-146b-5p, miR-129-5p vs. miR-132-3p, miR-146b-5p vs. miR-1-3p, and miR-146b-5p

ARTICLE IN PRESS

vs. miR-132-3p), while others were not (miR-129-5p vs. miR-1-3p, and miR-132-3p vs. miR-1-3p) **(Fig. 3c)**. Further, we noticed that mature miRNAs obtained from the parental precursors (pre-miRNAs) are positively correlated (high abundance miR-129-5p vs. low abundance miR-129-1-3p and high abundance miR-132-3p vs. low abundance miR-132-5p) **(Fig. 3d)**.

Differential miRNA expression in temporal cortex region in AD patients- Validation by RT-qPCR

To validate our findings, we employed RT-qPCR to measure the relative levels of NGS identified miRNAs: miR-129-5p, miR-146b-5p, miR-151a-5p, miR-1-3p, miR-132-3p, miR-18a-5p, miR-132-5p, miR-133a-3p, miR-151b, miR-3065-3p, and miR-129-1-3p. In this analysis, we did not assess the levels of novel-miR-71 and novel-miR-122, as they were not annotated for humans in miRBase database (the archive for microRNA sequences and annotations)[27] and lacked prior evidence in the PubMed database. The box plot in **Fig. 4a** illustrates the differential expression of these 11 miRNAs between the control and AD subjects. When we quantified the 5 miRNAs identified as highly abundant and differentially expressed (through NGS analysis), we observed lower expression for miR-129-5p, miR-146b-5p, miR-1-3p, and miR-132-3p in AD compared to the control group. Conversely, we found higher expression for miR-151a-5p in AD, although the difference was not statistically significant. Similarly, among the low abundance miRNAs, miR-132-5p, miR-133a-3p, and miR-129-1-3p exhibited lower expression in AD, while miR-18a-5p, miR-151b, and miR-3065-3p showed higher expression in AD. This finding is consistent with the NGS data. However, for miR-151b, miR-3065-3p, and miR-129-1-3p, the difference was not statistically significant **(Fig. 4a)**. Importantly, the correlation between the high abundance miRNAs expression shown in **supplementary Fig. 2a** is similar to the NSG data as in **Fig. 3a**. Next, in addition to small RNA U6 normalizer, we used miRNA normalizers identified based on NGS data from both control and AD individuals. We selected normalizer miR-16-5p (padj=0.56), that is abundantly expressed and another normalizer miR-30b-5p (padj=0.99), that is in similar levels of expression to miR-129-5p, miR-146b-5p, miR-151a-5p, miR-1-3p, and miR-132-3p **(Fig. 4b)**. In subsequent analysis we noticed a slight negative correlation between RIN and Ct values for U6 in AD patients **(Fig. 4c)**. A similar negative correlation was seen for other small RNA RNU5G **(Supplementary Fig. 2b)** but not for miRNAs: miR-16-5p and miR-30b-5p **(Fig. 4c)**. We used all three different normalizers U6, miR-16-5p and miR-30b-5p and noticed the same direction of fold changes. Notably, significant differences were obtained for all 5 miRNAs using miR-30b-5p as a normalizer **(Fig. 4d).** Moreover, when analysing all 36 samples, regardless of RIN values (control, n = 13; AD, n = 23) **(Table 1)**, RT-qPCR confirmed that the direction of miRNA expression changes remained consistent. Of note, significant differences were obtained for miR-129-5p, miR-146b-5p, and miR-132-3p and similar trend was obtained for miR-151a-5p ($p = 0.305$), miR-1-3p ($p = 0.139$) using miR-30b-5p as normalizer **(Supplementary Fig. 2c)**. This observation is in line with NGS data **(Fig. 2)** and RT-qPCR data **(Fig. 4a)** from the 19 samples whose RIN values ≥ 3.5. Collectively, the results from RT-qPCR provide additional evidence supporting the differential expression of specific miRNAs in individuals with AD compared to the control group.

miRNA association with tau pathology

The samples used in the study were more comprehensively characterized for neuropathological tau pathology, with Braak staging data available for all 19 samples, compared to amyloid pathology, for which Thal staging data is available for only 13 samples **(Table 1)**. Notably, Thal staging data is missing for 5 out of the 10 AD samples. Therefore, we sought to explore the relationship between miRNA expression (normalized counts from NGS and fold change values from RT-qPCR) and the Braak stages of tau pathology

ARTICLE IN PRESS

in 9 control and 10 AD cases. We found decreased expression of miR-129-5p, miR-146b-5p, and miR-132-3p as the disease progressed through Braak stages, whereas no significant differences were observed for miR-151a-5p and miR-1-3p **(Fig 5).** In addition, we performed an immunodetection of phosphorylated tau (pS396/S404) by PHF1 antibody on western blots of RIPA-soluble fraction of T1 isocortex brain homogenates. There was negligible amount of PHF1 immunodetection in control compared to AD **(Fig. 6a).** Densitometric analysis of PHF1 signal and the Braak stages are positively correlated and importantly they correlate with differentially expressed miRNAs in a similar manner **(Fig. 6b-c)**. Braak stages and densitometric analysis of PHF1 were negatively correlated with miR-129-5p, miR-146b-5p, and miR-132-3p and positively correlated with miR-151a-5p **(Fig. 6d-e)**. When assessed only in AD cases (Braak stages V and VI), no correlation was observed, suggesting similar pathology between stages V and VI **(Supplementary Fig. 3).** Taken together, we confirm that expression of miR-129-5p, miR-146b-5p, and miR-132-3p are associated with tau pathology progression.

miRNA mediated effect on seeding activity of pathological tau in HEK biosensor cells

To evaluate the potential modulating effects of miRNA in tau seeding, we analysed the fluorescence resonance energy transfer (FRET) signal by flow cytometry in HEK tau biosensor cells. For this, we first prepared sarkosyl-insoluble brain fractions from both control and AD patients, as shown in **Fig. 7a**. Next, we characterized the PHF tau species in these fractions using negative staining with electron microscopy **(Fig. 7b)**. The presence of PHF tau in the sarkosyl-insoluble fractions from AD brain was confirmed through western blotting with phospho-tau and total tau antibodies **(Fig. 7c)**. The sarkosyl-insoluble fraction from control brain showed no signal of phospho-tau or tau (**Fig. 7c**). Using HEK tau biosensor cells when assessed via flow cytometry, based on FRET, we detected no seeding induced by sarkosyl-insoluble control brain fractions. However, we observed a strong seeding induction by AD sarkosyl-insoluble fractions **(Fig. 7d).** Subsequently, we investigated the impact of 5 miRNAs with high abundance (miR-129-5p, miR-146b-5p, miR-151a-5p, miR-1-3p, and miR-132-3p) on modulating tau seeding by treating cells with miRNAs and AD sarkosyl-insoluble fractions followed by an analysis by flow cytometry. We found that the miR-146b-5p mimic enhanced tau seeding activity of AD fractions, while the miR-146b-5p inhibitor reduced this tau seeding activity. In contrast, the miR-151a-5p mimic reduced tau seeding activity of AD fractions, whereas the miR-151a-5p inhibitor enhanced tau seeding activity of AD fractions **(Fig. 7e-f).** Other miRNAs showed no striking modulation in tau seeding **(Fig. 7e)**. These effects were further confirmed through microscopy, showing comparable FRET signals for miR-146b-5p and miR-151a-5p (mimics and inhibitors) in HEK tau biosensor cells **(Fig. 7g).**

miRNA targets and pathway analysis

We retrieved targets for differentially downregulated miRNAs (miR-129-5p, miR-146b-5p, miR-132-5p, miR-133a-3p, miR-1-3p, miR-132-3p, and miR-129-1-3p) and differentially upregulated miRNAs (miR-18a-5p, miR-151a-5p, miR-151b, and miR-3065-3p) in AD, using miRNet web-based tool (https://www.mirnet.ca/)[37]. Targets predicted for downregulated miRNAs were involved in the KEGG pathways such as Neurotrophin signaling pathway, Dopaminergic synapse, Axon guidance, Long-term depression, Serotonergic synapse, Cholinergic synapse, and AD, with FDR < 0.05, among other predicted pathways **(Fig. 8a and b)**. Targets predicted for upregulated miRNAs did not reach significance with FDR < 0.05 for neuron-related pathways **(Fig. 8a)**. Importantly, targets such as *BID, CALM1, GNAQ, CALM2, CALM3, CAPN1, FADD, LRP1, PLCB3, GSK3B, CASP3, CASP9*, and *CDK5R1* were predicted for downregulated miRNAs in the AD pathways **(Fig. 8b and Supplementary Table 2)**. A list of targets and a number of

ARTICLE IN PRESS

pathway-specific targets for downregulated miRNAs in these enriched KEGG pathways was shown **(Supplementary Table 2 and Supplementary Fig. 4)**. Collectively, we provide a predictive miRNA-target network demonstrating that several targets involved in neuronal regulation and AD pathways could be regulated by these identified differentially expressed miRNAs.

Discussion

In this study, we employed two different methods to analyse differentially expressed miRNAs in post-mortem brain cortical samples from two different brain banks, Neuro-CEB (France) and ULB LHNN (Belgium): small RNA sequencing for high-throughput screening and RT-qPCR for validation of selected miRNAs. The RNA quality of subjects, as judged from their RIN, was variable but comparable to the quality reported in other studies of post-mortem human brain samples[20,39]. Importantly, consistent with other studies[42,45] we found no correlation between RNA quality (RIN) and miRNA expression. We identified by NGS that 13 miRNAs were differentially expressed in AD versus control. Among them, 8 were downregulated and 5 were upregulated in AD. Furthermore, in the RT-qPCR method, we used several normalizers to validate the consistent direction in fold changes for these NGS identified miRNAs. This process reinforces the reliability of our results and reduces potential biases related to variability in normalization conditions. Our results corroborate previously reported alteration of miRNA expression in AD brains[20,42,46], while also uncovering additional miRNAs that may play critical roles in AD pathophysiology. In addition, we did not observe any significant difference in miR-125b-5p expression between AD and control **(Supplementary Fig. 5)** despite its identification as a promising upregulated miRNA in AD by meta-analysis[15]. This finding supports a recent study suggesting that miR-125b-5p may be less relevant in AD pathogenesis[20]. Notably, our study, using an independent cohort, demonstrates that the consistent downregulation of these miRNAs (miR-132, miR-129-5p, and miR-146b-5p) aligns with the findings from a recent large-scale miRNA profiling study in AD using the ROS/MAP cohort[47]. Furthermore, the downregulation miR-132, miR-129-5p, and miR-146b-5p was associated with other age-related cerebral pathologies, suggesting a shared mechanism involved in those pathologies[47].

Among differentially expressed miRNAs of high abundance, the expression of several of them was also negatively or positively correlated between them. The lack of any significant correlation of RIN or PMD with the miRNA expressions, reinforces that these correlative changes in expression levels reflect a consistent miRNAs dysregulation. In line with our data, a similar positive correlation between two AD downregulated miRNAs, miR-129-5p vs. miR-132-3p was shown in ROSMAP study[48]. We observed that the level of 3p and 5p mature miRNAs obtained from pre-miRNAs (for miR-132 and miR-129) are positively correlated. Strikingly, similar to our observation, such a positive correlation between miR-132-3p and miR-132-5p mature miRNAs obtained from the same precursor, miR-132, has been shown in brain regions of frontotemporal dementia[49].

Some of the 13 miRNAs that we identified as differentially expressed miRNAs have been reported as such in several studies **(Table 2).** For instance, miR-132-3p, miR-132-5p, miR-129-5p, and miR-129-1-3p have been found to be downregulated in several regions of the AD brain. We previously highlighted that miR-132 and miR-129 are frontrunner miRNAs downregulated in AD[50]. Not only in brain regions, but also in the CSF of AD patients, miR-132-3p and miR-129-5p were reported to be downregulated[51]. Some other miRNAs, such as miR-146b-5p, miR-18a-5p, and miR-1-3p, were reported to be dysregulated in AD at least once. In our study, we observed downregulation of miR-146b-5p. While several studies reported an upregulation of miR-146a-5p in AD brains[10,15], miR-146b-5p was observed to be downregulated in a few

ARTICLE IN PRESS

studies[52-54]. In line with observations in the brain, a study in CSF showed that miR-146b-5p decreased in AD[52]; furthermore, another study in CSF shows a trend toward its decline in AD compared to control and MCI[55]. We also found a declining trend for miR-146b-5p in the brain, showing that as Braak stages increase, miR-146b-5p decreases **(Fig. 5)**. Additionally, in whole blood from the Australian Imaging Biomarkers Lifestyle Study of Ageing (AIBL) cohort, miR-146b-5p was downregulated in AD compared to control[56]. miR-18a-5p, miR-151a-5p, and miR-3065-3p were upregulated in our study, consistent with the reported upregulation of these miRNAs in the AD brain[42,54]. miR-151a-5p and miR-151b were shown to be upregulated in AD CSF[52]. Contrastingly, miR-18a-5p and miR-151a-5p were shown to be downregulated in AD compared to control in the plasma of Polish cohorts[57]. miR-3065-3p was upregulated in the serum exosome of AD patients compared to non-demented control[54]. miR-1-3p was downregulated in our study, while another study using samples from the inferior frontal gyrus and superior temporal gyrus reported upregulation of miR-1-3p [58].

In terms of functional relevance, miR-132 is one of the better-characterized miRNAs and has been shown to exert protective effects by targeting multiple signaling pathways involved in amyloid[59,60] and tau pathology[16], neurogenesis and memory formation[61]. Computational analyses have identified miR-129-5p as a potential biomarker for both neuropathology and cognitive decline in AD[62]. Furthermore, a recent study using mouse primary neuronal mixed (PNM) cultures demonstrated that reduced levels of miR-129-5p in astrocytes exacerbate inflammatory processes and impair neuronal support functions[63]. Additionally, miR-151 has been implicated in hippocampal contextual fear memory formation through its regulation of the anterior pharynx-defective 1a (APH1a) protein[64]. In cellular models, miR-146b-5p has been shown to target TRAF6 and is therefore suggested to attenuate neuroinflammation[65].

An interesting feature of our study is that we used brain specimens from the same individuals for both miRNA expression analysis and phospho-tau assessment. This allowed us to precisely evaluate the association between miRNA dysregulation and phospho-tau quantification. Analysis of the association between miRNA expression and tau pathology revealed that Braak stages and PHF1 densitometric values were negatively correlated with miR-129-5p, miR-146b-5p, and miR-132-3p, but positively correlated with miR-151a-5p. The neuroprotective effects of miR-132-3p against tau pathology have been reported in a few studies[16,66]. However, in our experimentation using an *in vitro* HEK tau biosensor cells, we did not observe a decrease in tau aggregation based on FRET signaling. The same applies to miR-129-5p, another downregulated miRNA in AD. When testing other miRNAs, the miR-146b-5p mimic increased tau seeding, while its inhibitor decreased it. In contrast, the miR-151a-5p mimic decreased tau seeding, but its inhibitor increased it. Furthermore, in the search for predicted targets of miR-146b-5p, we identified sortilin 1 (*SORT1*) as one of the top 10 predicted targets of miR-146b-5p (https://mirdb.org/index.html)[67]. SORT1 is involved in lysosomal degradation of ligands after binding and internalization[68,69]. One study reported that blocking SORT1 with antibodies in forebrain homogenates derived from mice expressing the P301S mutation in the *MAPT* gene reduced its inhibition of tau seeding in HEK tau biosensor cells[70]. Therefore, in HEK tau biosensor cells, which also harbour the P301S mutation, upregulation of the miR-146b-5p mimic could downregulate SORT1 and thereby enhance tau seeding. Whether this mechanism, or other yet unidentified mechanisms, underlies the observed promotion of tau seeding by the miR-146b-5p mimic in HEK tau biosensor cells needs to be validated. In the case of miR-151a-5p, it is known to reduce cellular ATP[71], and ATP kinetically induces tau filament formation[72,73]. Therefore, we hypothesize that an increase in miR-151a-5p could reduce cellular ATP, which in turn would reduce tau seeding and thereby lower the FRET signals. Most importantly, it remains to be determined whether the increase in miR-151a-5p and the

ARTICLE IN PRESS

decrease in miR-146b-5p in the AD brain represent a protective mechanism as the disease progresses. Nevertheless, miRNAs are multi-targeting molecules. High-throughput transcriptomic and proteomic analyses will be needed to reveal potential targets of miR-146b-5p and miR-151a-5p involved in tau-related pathways. While these findings are notable, FRET results must be interpreted cautiously: HEK tau biosensor cells are non-neuronal, lack full-length tau, and represent a single cell type. For instance, in brain-related cells, miR-146b-5p suppresses glial inflammation[65,74], while its loss increases neuronal proliferation in vivo[75]. However, this phenomenon cannot be studied in HEK tau biosensor cells. Furthermore, mixed cultures better reflect intercellular interactions, as responses of one cell type in which miRNA is dysregulated can affect another[63]. This needs to be evaluated in neuronal and inflammatory mixed cultures for further investigation.

Additionally, with respect to therapeutics, it is important to identify the targets and signaling pathways that may be influenced by these identified miRNAs. The miRNA-target network analysis revealed that targets for downregulated miRNAs in AD are associated with KEGG pathways such as the Neurotrophin signaling pathway, Dopaminergic synapse, Axon guidance, Long-term depression, Serotonergic synapse, Cholinergic synapse, and AD. Some of these miRNA-target relationships need to be validated in AD-relevant models. For instance, miR-132-3p, a well-documented downregulated miRNA in AD that we also identified in this study, is known to exert protective effects by modulating multiple pathways[16,61]. This highlights the potential of replacement therapy, where restoring these miRNAs could confer beneficial effects. From a diagnostic perspective, their levels should be systematically investigated in large cohorts using biofluids such as CSF and blood, particularly those derived from the brain, and correlated with conventional AD biomarkers, including total tau (t-tau), phosphorylated tau (p-tau), amyloid-beta (Aβ), and cognitive scores.

We acknowledge that there are limitations in our study. First, for identifying the differentially expressed miRNAs, we used Braak stages 0–III as controls and Braak stages V–VI as AD; the damage to cells and tissues is higher at Braak stages V–VI. We cannot exclude the possibility that cell or tissue loss at stages V–VI could influence these miRNA profiles. Larger cohort studies with equal numbers of Braak stages within 0–IV will be necessary to track miRNA changes within Braak stages 0–IV, before the pathology becomes aggressive. Furthermore, some AD patients have comorbid conditions, and larger studies with distinct groups will be needed to identify the most specific AD miRNA signatures. Second, our sequencing analysis included only 19 of 36 samples, limiting statistical power. We applied an FDR <0.1, which is less stringent than the conventional <0.05. Although none of the miRNAs reached the conventional FDR <0.05 threshold, their consistent reporting in previous studies **(Table 2)**, together with their substantial fold changes, supports their potential relevance to AD. The lack of significance is likely attributable to our limited sample size. Moreover, when sex is included as confounding factor, we lost the significance at the cut off used nominal p value <0.003 and FDR <0.1 **(Supplementary Table 3).** This could be due to large gender imbalance (control group: n=9; 8 males and 1 female, and AD group: n=10; 3 males and 7 females) and small cohort size. The effect of other confounding factors such as age, PMD, RIN were minimal compared to sex **(Supplementary Table 3).** Analysis of all 36 samples from **Table 1** (control group: n=13; 9 males and 4 females; AD group: n=23; 11 males and 12 females) by RT-qPCR confirmed that miR-132-3p, miR-146b-5p, and miR-129-5p were downregulated in AD **(Supplementary Fig. 2c)**. Supporting our findings, a recent large cohort study - Religious Orders Study (ROS) or the Rush Memory and Aging Project (MAP) with cohort size of n=617, revealed that some of the differential expression of miRNAs we observed (miR-132-3p, miR-132-5p, miR-146b-5p, miR-129-1-3p, and miR-129-5p) even after adjusting for sex, age, education, PMI, RIN, batch, surrogate variables, and co-occurring pathologies at FDR adjusted p value

ARTICLE IN PRESS

<0.05[47]. Thus, we considered to be appropriate to study these miRNAs but acknowledge that further experiments are needed to prove their relevance for AD. Third, some of the information on clinical and neuropathological diagnoses were lacking. Although we had complete diagnostic information for tau pathology (Braak staging), data on amyloid pathology (Thal staging) were not available for all samples in our cohort. Consequently, our analysis focused exclusively on evaluating the association between differential miRNA expression and tau pathology, using Braak staging and phosphorylated tau quantification. Nevertheless, based on the available Thal staging data for amyloid pathology (13 out of 19 subjects used for sequencing), we observed a similar correlation between Thal staging and miRNA expression as seen with tau pathology **(Supplementary Fig. 6)**. This observation aligns with previous findings reporting that miR-132-3p and miR-129-5p in the brain are associated with both amyloid and tau pathology[48]. Given that miRNAs can target multiple genes and influence multiple biological pathways, we do not exclude the possibility that these identified differentially expressed miRNAs also contribute to amyloid pathology. Our study lacks experimental evidence directly linking the identified miRNAs to amyloid pathology. A literature search revealed that among the identified miRNAs, miR-132-3p has been associated with amyloid pathology in mouse models. One study demonstrated that deletion of miR-132/212 promoted Aβ production and amyloid plaque formation in the brains of 3xTg-AD mice[60]. Similarly, in APP/PS1 mice, intracerebroventricular injection of antagomiR-132 increased amyloid plaque burden[19]. Supporting this finding, another study showed that overexpression of miR-132-3p reduced amyloid plaque formation in the hippocampus of APP/PS1 mice[59]. Further studies involving larger, well-characterized cohorts encompassing both pathological features, along with experimental models representing both combined and distinct pathologies, are needed to elucidate the associations and regulatory roles of these identified differentially expressed miRNAs. Additionally, patient diagnostic data during disease development, such as cognitive scores and CSF biomarkers, were lacking in our cohort; therefore, no association study with miRNA expression was possible. Lastly, our analysis was based on bulk sequencing. Future studies using single-cell sequencing are necessary to identify the specific cellular sources of these miRNAs. Despite these limitations, this study provides valuable information on the alteration of miRNA levels in human post-mortem AD brains and their implications in tau seeding. Further studies in other models are needed to better understand their regulatory roles in tau pathology.

In conclusion, our study corroborates the previously reported dysregulation of miRNAs in AD and identifies additional dysregulated miRNAs in AD brain tissue. In particular, miR-129-5p, miR-146b-5p, miR-132-3p, and miR-151a-5p expression showed association with tau pathology in AD brains. However, only miR-146b-5p and miR-151a-5p showed an effect on tau seeding in cultured cells suggesting a direct role of these miRNAs in tau pathology formation. Their mechanisms of action are yet to be fully resolved, and additional studies will help to understand their involvement in AD pathology and may lead to strategies to treat this devastating disease.

Acknowledgements

The post-mortem brain samples were provided by the brain bank of Neuro-CEB Neuropathology network (funded by ARSLA, CSC, France DFT, Fondation France SEP, Fondation Vaincre Alzheimer, France Parkinson, PSP France) and brain bank of ULB LHNN, Belgium (BB190052). We thank the members of the NeuroCEB Neuropathology network : Dr. Franck Letournel (CHU Angers), Dr. Marie-Laure Martin-Négrier (CHU Bordeaux), Dr. Maxime Faisant (CHU Caen), Prof. Catherine Godfraind (CHU Clermont-Ferrand), Prof. Claude-Alain Maurage (CHU Lille), Dr. Vincent Deramecourt (CHU Lille), Dr. Mathilde Duchesne (CHU Limoges), Dr. David Meyronnet (CHU Lyon), Dr. Clémence Deltei (CHU Marseille), Prof. Valérie Rigau (CHU

ARTICLE IN PRESS

Montpellier), Dr. Fanny Vandenbos-Burel (Nice), Prof. Danielle Seilhean (CHU PS, Paris), Dr. Susana Boluda (CHU PS, Paris), Dr. Isabelle Plu (CHU PS, Paris), Dr. Dan Christian Chiforeanu (CHU Rennes), Dr. Florent Marguet (CHU Rouen), Dr. Béatrice Lannes (CHU Strasbourg). We thank Dr. Peter Davis (The Feinstein Institute for Medical Research, New York) for PHF1 antibody. We sincerely thank Dr. Sabrina Turbant for brain tissue preparation, Prof. Miriam Cnop and Prof. Decio L. Eizirik for helpful discussions, and Mrs. Christine Dubois (ULB flow cytometry platform) for technical help. This study was supported by the Belgian FNRS (S.N, C.Q.-S, K.A, L.L.-G, A.-C.K) and fundings from Fondation Recherche Alzheimer/ Stichting Alzheimer Onderzoek (S.N. 2021/0028, S.N. 2023/0025), the Belgian Fonds de la Recherche Scientifique Médicale (T.0023.15) (J.-P.B), the Fund Aline (King Baudoin Foundation, 14001) (J.-P.B), the Fondation Médicale Reine Elisabeth (K.L), the ULB Génicot Fund (J.-P.B and K.L), Simone and Pierre Clerdent prize (K.L) and the Jaumotte-Demoulin Fund (K.L).

Author contributions

S.N, J.-P. B and K.L contributed to the conception and design of the study. S.N, C.Q.-S, K.A, L.L.-G, E.D, A.-C.K, E.A carried out the experiments. Y.G, F.V.N performed miRNA sequencing, Y.G, F.V.N, S.N and C.Q.-S performed data analysis. J.-P. B contributed to the collection and sample preparation of some of the post-mortem human brain tissues. S.N and K.L drafted the manuscript. All authors contributed to manuscript revision and approved the submitted version.

Competing interests

The authors declare that they have no competing interests.

References

1 Nandi, A. *et al.* Global and regional projections of the economic burden of Alzheimer's disease and related dementias from 2019 to 2050: A value of statistical life approach. *EClinicalMedicine* **51**, 101580, doi:10.1016/j.eclinm.2022.101580 (2022).

2 Congdon, E. E. & Sigurdsson, E. M. Tau-targeting therapies for Alzheimer disease. *Nature reviews. Neurology* **14**, 399-415, doi:10.1038/s41582-018-0013-z (2018).

3 Panza, F., Lozupone, M., Logroscino, G. & Imbimbo, B. P. A critical appraisal of amyloid-β-targeting therapies for Alzheimer disease. *Nat Rev Neurol* **15**, 73-88, doi:10.1038/s41582-018-0116-6 (2019).

4 Jack, C. R. *et al.* NIA-AA Research Framework: Toward a biological definition of Alzheimer's disease. *Alzheimers Dement* **14**, 535-562, doi:10.1016/j.jalz.2018.02.018 (2018).

5 Brion, J. P. *et al.* Tau in Alzheimer neurofibrillary tangles. N- and C-terminal regions are differentially associated with paired helical filaments and the location of a putative abnormal phosphorylation site. *Biochem J* **273(Pt 1)**, 127-133, doi:10.1042/bj2730127 (1991).

6 Vergara, C. *et al.* Amyloid-β pathology enhances pathological fibrillary tau seeding induced by Alzheimer PHF in vivo. *Acta Neuropathol* **137**, 397-412, doi:10.1007/s00401-018-1953-5 (2019).

7 Cummings, J. & Fox, N. Defining Disease Modifying Therapy for Alzheimer's Disease. *J Prev Alzheimers Dis* **4**, 109-115, doi:10.14283/jpad.2017.12 (2017).

8 Golde, T. E. Disease-Modifying Therapies for Alzheimer's Disease: More Questions than Answers. *Neurotherapeutics* **19**, 209-227, doi:10.1007/s13311-022-01201-2 (2022).

9 Idda, M. L., Munk, R., Abdelmohsen, K. & Gorospe, M. Noncoding RNAs in Alzheimer's disease. *Wiley Interdiscip Rev RNA* **9**, doi:10.1002/wrna.1463 (2018).

ARTICLE IN PRESS

ARTICLE IN PRESS

10 Nagaraj, S., Zoltowska, K. M., Laskowska-Kaszub, K. & Wojda, U. microRNA diagnostic panel for Alzheimer's disease and epigenetic trade-off between neurodegeneration and cancer. *Ageing Res Rev* **49**, 125-143, doi:10.1016/j.arr.2018.10.008 (2019).

11 Lauretti, E., Dabrowski, K. & Praticò, D. The neurobiology of non-coding RNAs and Alzheimer's disease pathogenesis: Pathways, mechanisms and translational opportunities. *Ageing Res Rev* **71**, 101425, doi:10.1016/j.arr.2021.101425 (2021).

12 Bartel, D. P. Metazoan MicroRNAs. *Cell* **173**, 20-51, doi:10.1016/j.cell.2018.03.006 (2018).

13 Nagaraj, S. *et al.* Candidate Alzheimer's Disease Biomarker miR-483-5p Lowers TAU Phosphorylation by Direct ERK1/2 Repression. *Int J Mol Sci* **22**, doi:10.3390/ijms22073653 (2021).

14 Chopra, N. *et al.* MicroRNA-298 reduces levels of human amyloid-β precursor protein (APP), β-site APP-converting enzyme 1 (BACE1) and specific tau protein moieties. *Mol Psychiatry* **26**, 5636-5657, doi:10.1038/s41380-019-0610-2 (2021).

15 Takousis, P. *et al.* Differential expression of microRNAs in Alzheimer's disease brain, blood, and cerebrospinal fluid. *Alzheimers Dement* **15**, 1468-1477, doi:10.1016/j.jalz.2019.06.4952 (2019).

16 El Fatimy, R. *et al.* MicroRNA-132 provides neuroprotection for tauopathies via multiple signaling pathways. *Acta Neuropathol* **136**, 537-555, doi:10.1007/s00401-018-1880-5 (2018).

17 Banzhaf-Strathmann, J. *et al.* MicroRNA-125b induces tau hyperphosphorylation and cognitive deficits in Alzheimer's disease. *EMBO J* **33**, 1667-1680, doi:10.15252/embj.201387576 (2014).

18 Sun, T. *et al.* miR-30a-5p induces Aβ production via inhibiting the nonamyloidogenic pathway in Alzheimer's disease. *Pharmacol Res* **178**, 106153, doi:10.1016/j.phrs.2022.106153 (2022).

19 Salta, E., Sierksma, A., Vanden Eynden, E. & De Strooper, B. miR-132 loss de-represses ITPKB and aggravates amyloid and TAU pathology in Alzheimer's brain. *EMBO Mol Med* **8**, 1005-1018, doi:10.15252/emmm.201606520 (2016).

20 Dobricic, V. *et al.* Differential microRNA expression analyses across two brain regions in Alzheimer's disease. *Transl Psychiatry* **12**, 352, doi:10.1038/s41398-022-02108-4 (2022).

21 Hyman, B. T. & Trojanowski, J. Q. Consensus recommendations for the postmortem diagnosis of Alzheimer disease from the National Institute on Aging and the Reagan Institute Working Group on diagnostic criteria for the neuropathological assessment of Alzheimer disease. *J Neuropathol Exp Neurol* **56**, 1095-1097, doi:10.1097/00005072-199710000-00002 (1997).

22 Braak, H. & Braak, E. Neuropathological stageing of Alzheimer-related changes. *Acta neuropathologica* **82**, 239-259, doi:10.1007/BF00308809 (1991).

23 Thal, D. R., Rub, U., Orantes, M. & Braak, H. Phases of A beta-deposition in the human brain and its relevance for the development of AD. *Neurology* **58**, 1791-1800 (2002).

24 Smith, T., Heger, A. & Sudbery, I. UMI-tools: modeling sequencing errors in Unique Molecular Identifiers to improve quantification accuracy. *Genome Res* **27**, 491-499, doi:10.1101/gr.209601.116 (2017).

25 Wingett, S. W. & Andrews, S. FastQ Screen: A tool for multi-genome mapping and quality control. *F1000Res* **7**, 1338, doi:10.12688/f1000research.15931.2 (2018).

26 Shi, J. *et al.* mirPRo-a novel standalone program for differential expression and variation analysis of miRNAs. *Sci Rep* **5**, 14617, doi:10.1038/srep14617 (2015).

27 Kozomara, A., Birgaoanu, M. & Griffiths-Jones, S. miRBase: from microRNA sequences to function. *Nucleic Acids Res* **47**, D155-D162, doi:10.1093/nar/gky1141 (2019).

28 Chen, Y., Chen, L., Lun, A. T. L., Baldoni, P. L. & Smyth, G. K. edgeR v4: powerful differential analysis of sequencing data with expanded functionality and improved support for small counts and larger datasets. *Nucleic Acids Res* **53**, doi:10.1093/nar/gkaf018 (2025).

ARTICLE IN PRESS

ARTICLE IN PRESS

29 Livak, K. J. & Schmittgen, T. D. Analysis of relative gene expression data using real-time quantitative PCR and the 2(-Delta Delta C(T)) Method. *Methods* **25**, 402-408, doi:10.1006/meth.2001.1262 (2001).

30 Ando, K. *et al.* Alteration of gene expression and protein solubility of the PI 5-phosphatase SHIP2 are correlated with Alzheimer's disease pathology progression. *Acta Neuropathol* **147**, 94, doi:10.1007/s00401-024-02745-7 (2024).

31 Ando, K. *et al.* Vaccination with Sarkosyl insoluble PHF-tau decrease neurofibrillary tangles formation in aged tau transgenic mouse model: a pilot study. *J Alzheimers Dis* **40 Suppl 1**, S135-145, doi:10.3233/JAD-132237 (2014).

32 Ando, K. *et al.* Accelerated human mutant tau aggregation by knocking out murine tau in a transgenic mouse model. *The American journal of pathology* **178**, 803-816, doi:10.1016/j.ajpath.2010.10.034. (2011).

33 Ando, K. *et al.* The lipid phosphatase Synaptojanin 1 undergoes a significant alteration in expression and solubility and is associated with brain lesions in Alzheimer's disease. *Acta Neuropathol Commun* **8**, 79, doi:10.1186/s40478-020-00954-1 (2020).

34 Greenberg, S. G., Davies, P., Schein, J. D. & Binder, L. I. Hydrofluoric acid-treated tau PHF proteins display the same biochemical properties as normal tau. *The Journal of biological chemistry* **267**, 564-569 (1992).

35 Holmes, B. B. *et al.* Proteopathic tau seeding predicts tauopathy in vivo. *Proceedings of the National Academy of Sciences of the United States of America* **111**, E4376-4385, doi:10.1073/pnas.1411649111 (2014).

36 de Fisenne, M. A. *et al.* Alzheimer PHF-tau aggregates do not spread tau pathology to the brain via the Retino-tectal projection after intraocular injection in male mouse models. *Neurobiology of disease* **174**, 105875, doi:10.1016/j.nbd.2022.105875 (2022).

37 Chang, L., Zhou, G., Soufan, O. & Xia, J. miRNet 2.0: network-based visual analytics for miRNA functional analysis and systems biology. *Nucleic Acids Res* **48**, W244-W251, doi:10.1093/nar/gkaa467 (2020).

38 Kanehisa, M. & Goto, S. KEGG: kyoto encyclopedia of genes and genomes. *Nucleic Acids Res* **28**, 27-30, doi:10.1093/nar/28.1.27 (2000).

39 Wingo, A. P. *et al.* Brain microRNAs are associated with variation in cognitive trajectory in advanced age. *Transl Psychiatry* **12**, 47, doi:10.1038/s41398-022-01806-3 (2022).

40 Annese, A. *et al.* Whole transcriptome profiling of Late-Onset Alzheimer's Disease patients provides insights into the molecular changes involved in the disease. *Sci Rep* **8**, 4282, doi:10.1038/s41598-018-22701-2 (2018).

41 Hébert, S. S., Wang, W. X., Zhu, Q. & Nelson, P. T. A study of small RNAs from cerebral neocortex of pathology-verified Alzheimer's disease, dementia with lewy bodies, hippocampal sclerosis, frontotemporal lobar dementia, and non-demented human controls. *J Alzheimers Dis* **35**, 335-348, doi:10.3233/JAD-122350 (2013).

42 Lau, P. *et al.* Alteration of the microRNA network during the progression of Alzheimer's disease. *EMBO Mol Med* **5**, 1613-1634, doi:10.1002/emmm.201201974 (2013).

43 Wang, W. X., Huang, Q., Hu, Y., Stromberg, A. J. & Nelson, P. T. Patterns of microRNA expression in normal and early Alzheimer's disease human temporal cortex: white matter versus gray matter. *Acta Neuropathol* **121**, 193-205, doi:10.1007/s00401-010-0756-0 (2011).

44 Hébert, S. S. *et al.* Loss of microRNA cluster miR-29a/b-1 in sporadic Alzheimer's disease correlates with increased BACE1/beta-secretase expression. *Proc Natl Acad Sci U S A* **105**, 6415-6420, doi:10.1073/pnas.0710263105 (2008).

45 Dobricic, V. *et al.* Common signatures of differential microRNA expression in Parkinson's and Alzheimer's disease brains. *Brain Commun* **4**, fcac274, doi:10.1093/braincomms/fcac274 (2022).

ARTICLE IN PRESS

ARTICLE IN PRESS

46 Pichler, S. *et al.* The miRNome of Alzheimer's disease: consistent downregulation of the miR-132/212 cluster. *Neurobiol Aging* **50**, 167.e161-167.e110, doi:10.1016/j.neurobiolaging.2016.09.019 (2017).

47 Luo, T. *et al.* Brain microRNAs differentially expressed in age-related cerebral pathologies. *Neurobiol Aging* **151**, 42-53, doi:10.1016/j.neurobiolaging.2025.03.014 (2025).

48 Patrick, E. *et al.* Dissecting the role of non-coding RNAs in the accumulation of amyloid and tau neuropathologies in Alzheimer's disease. *Mol Neurodegener* **12**, 51, doi:10.1186/s13024-017-0191-y (2017).

49 Chen-Plotkin, A. S. *et al.* TMEM106B, the risk gene for frontotemporal dementia, is regulated by the microRNA-132/212 cluster and affects progranulin pathways. *J Neurosci* **32**, 11213-11227, doi:10.1523/JNEUROSCI.0521-12.2012 (2012).

50 Nagaraj, S. *et al.* Downregulation of hsa-miR-132 and hsa-miR-129: non-coding RNA molecular signatures of Alzheimer's disease. *Front Mol Neurosci* **17**, 1423340, doi:10.3389/fnmol.2024.1423340 (2024).

51 Burgos, K. *et al.* Profiles of extracellular miRNA in cerebrospinal fluid and serum from patients with Alzheimer's and Parkinson's diseases correlate with disease status and features of pathology. *PLoS One* **9**, e94839, doi:10.1371/journal.pone.0094839 (2014).

52 Cogswell, J. P. *et al.* Identification of miRNA changes in Alzheimer's disease brain and CSF yields putative biomarkers and insights into disease pathways. *J Alzheimers Dis* **14**, 27-41, doi:10.3233/jad-2008-14103 (2008).

53 Weinberg, R. B., Mufson, E. J. & Counts, S. E. Evidence for a neuroprotective microRNA pathway in amnestic mild cognitive impairment. *Front Neurosci* **9**, 430, doi:10.3389/fnins.2015.00430 (2015).

54 Cheng, L. *et al.* Small RNA fingerprinting of Alzheimer's disease frontal cortex extracellular vesicles and their comparison with peripheral extracellular vesicles. *J Extracell Vesicles* **9**, 1766822, doi:10.1080/20013078.2020.1766822 (2020).

55 Sandau, U. S. *et al.* Performance of Validated MicroRNA Biomarkers for Alzheimer's Disease in Mild Cognitive Impairment. *J Alzheimers Dis* **78**, 245-263, doi:10.3233/JAD-200396 (2020).

56 Wu, H. Z. Y. *et al.* Differential blood miRNA expression in brain amyloid imaging-defined Alzheimer's disease and controls. *Alzheimers Res Ther* **12**, 59, doi:10.1186/s13195-020-00627-0 (2020).

57 Nagaraj, S. *et al.* Profile of 6 microRNA in blood plasma distinguish early stage Alzheimer's disease patients from non-demented subjects. *Oncotarget* **8**, 16122-16143, doi:10.18632/oncotarget.15109 (2017).

58 Li, Q. S. & Cai, D. Integrated miRNA-Seq and mRNA-Seq Study to Identify miRNAs Associated With Alzheimer's Disease Using Post-mortem Brain Tissue Samples. *Front Neurosci* **15**, 620899, doi:10.3389/fnins.2021.620899 (2021).

59 Zeng, C., Meng, X., Mai, D., Xu, K. & Qu, S. Overexpression of miR-132-3p contributes to neuronal protection in in vitro and in vivo models of Alzheimer's disease. *Behav Brain Res* **417**, 113584, doi:10.1016/j.bbr.2021.113584 (2022).

60 Hernandez-Rapp, J. *et al.* microRNA-132/212 deficiency enhances Aβ production and senile plaque deposition in Alzheimer's disease triple transgenic mice. *Sci Rep* **6**, 30953, doi:10.1038/srep30953 (2016).

61 Walgrave, H. *et al.* Restoring miR-132 expression rescues adult hippocampal neurogenesis and memory deficits in Alzheimer's disease. *Cell Stem Cell* **28**, 1805-1821.e1808, doi:10.1016/j.stem.2021.05.001 (2021).

62 Han, S. W. *et al.* miR-129-5p as a biomarker for pathology and cognitive decline in Alzheimer's disease. *Alzheimers Res Ther* **16**, 5, doi:10.1186/s13195-023-01366-8 (2024).

ARTICLE IN PRESS

ARTICLE IN PRESS

63 Kaurani, L. *et al.* A role for astrocytic miR-129-5p in frontotemporal dementia. *Transl Psychiatry* **15**, 142, doi:10.1038/s41398-025-03338-y (2025).

64 Xu, X. F., Wang, Y. C., Zong, L. & Wang, X. L. miR-151-5p modulates APH1a expression to participate in contextual fear memory formation. *RNA Biol* **16**, 282-294, doi:10.1080/15476286.2019.1572435 (2019).

65 Liu, M. *et al.* MiR-146b-5p/TRAF6 axis is essential for *Ginkgo biloba* L. extract GBE to attenuate LPS-induced neuroinflammation. *Front Pharmacol* **13**, 978587, doi:10.3389/fphar.2022.978587 (2022).

66 Smith, P. Y. *et al.* miR-132/212 deficiency impairs tau metabolism and promotes pathological aggregation in vivo. *Hum Mol Genet* **24**, 6721-6735, doi:10.1093/hmg/ddv377 (2015).

67 Chen, Y. & Wang, X. miRDB: an online database for prediction of functional microRNA targets. *Nucleic Acids Res* **48**, D127-D131, doi:10.1093/nar/gkz757 (2020).

68 Nykjaer, A. & Willnow, T. E. Sortilin: a receptor to regulate neuronal viability and function. *Trends Neurosci* **35**, 261-270, doi:10.1016/j.tins.2012.01.003 (2012).

69 Uchiyama, K. *et al.* Prions amplify through degradation of the VPS10P sorting receptor sortilin. *PLoS Pathog* **13**, e1006470, doi:10.1371/journal.ppat.1006470 (2017).

70 Johnson, N. R. *et al.* Evidence for sortilin modulating regional accumulation of human tau prions in transgenic mice. *Proc Natl Acad Sci U S A* **114**, E11029-E11036, doi:10.1073/pnas.1717193114 (2017).

71 Zhou, R. *et al.* Mitochondria-related miR-151a-5p reduces cellular ATP production by targeting CYTB in asthenozoospermia. *Sci Rep* **5**, 17743, doi:10.1038/srep17743 (2015).

72 Heo, C. E. *et al.* ATP Kinetically Modulates Pathogenic Tau Fibrillations. *ACS Chem Neurosci* **11**, 3144-3152, doi:10.1021/acschemneuro.0c00479 (2020).

73 Farid, M., Corbo, C. P. & Alonso, A. e. C. Tau binds ATP and induces its aggregation. *Microsc Res Tech* **77**, 133-137, doi:10.1002/jemt.22319 (2014).

74 Thompson, C. E. *et al.* MiR-146b-5p Decreases Cytokine Release From Astrocytes and Preserves Oligodendrocyte Progenitor Cell Complexity During Inflammation. *Eur J Neurosci* **62**, e70248, doi:10.1111/ejn.70248 (2025).

75 Chithanathan, K. *et al.* Enhanced Cognition and Neurogenesis in miR-146b Deficient Mice. *Cells* **11**, doi:10.3390/cells11132002 (2022).

76 Wong, H. K. *et al.* De-repression of FOXO3a death axis by microRNA-132 and -212 causes neuronal apoptosis in Alzheimer's disease. *Hum Mol Genet* **22**, 3077-3092, doi:10.1093/hmg/ddt164 (2013).

77 Absalon, S., Kochanek, D. M., Raghavan, V. & Krichevsky, A. M. MiR-26b, upregulated in Alzheimer's disease, activates cell cycle entry, tau-phosphorylation, and apoptosis in postmitotic neurons. *J Neurosci* **33**, 14645-14659, doi:10.1523/JNEUROSCI.1327-13.2013 (2013).

Sample	Sample ID	Sex	Age (years)	PMD (hours)	RIN	A260 /A280	APOE status	Braak staging	Thal staging	Brain bank
CTR 1	3549	M	69	6	6.6	1.895	E2/E3	0	0	Neuro-CEB
CTR 2	4078	M	73	10	5.4	1.903	E3/E3	II	0	Neuro-CEB
CTR 3	8866	M	84	13.5	7.6	1.924	E3/E3	0	1	Neuro-CEB
CTR 4	3862	M	58	5.5	5.1	1.949	NA	III	0	Neuro-CEB
CTR 5	63	M	81	16.5	3.6	1.937	E3/E3	0	NA	ULB LHNN
CTR 6	87	M	67	24	4.7	1.881	E3/E3	I	0	ULB LHNN
CTR 7	65	F	77	48	3.5	1.87	E3/E4	III	4	ULB LHNN

ARTICLE IN PRESS

CTR 8	**75**	**M**	**71**	**24**	**3.7**	**1.943**	**E3/E4**	**III**	**2**	**ULB LHNN**
CTR 9	**88**	**M**	**69**	**24**	**4.4**	**1.942**	**E3/E4**	**III**	**3**	**ULB LHNN**
CTR 10	8401	F	60	28	2.6	1.889	E3/E3	0	0	Neuro-CEB
CTR 11	51	F	89	35	2.4	1.916	E2/E4	NA	NA	ULB LHNN
CTR 12	62	F	71	7	3	1.934	E3/E4	NA	NA	ULB LHNN
CTR 13	43	M	73	9.5	2.6	1.911	E3/E4	NA	NA	ULB LHNN
AD 1	**4570**	**M**	**64**	**3**	**7.1**	**1.918**	**E3/E3**	**VI**	**NA**	**Neuro-CEB**
AD 2	**3435**	**F**	**82**	**20.5**	**3.5**	**1.937**	**E3/E3**	**VI**	**NA**	**Neuro-CEB**
AD 3	**8010**	**F**	**83**	**24**	**7.3**	**1.926**	**E3/E3**	**VI**	**5**	**Neuro-CEB**
AD 4	**58**	**F**	**81**	**8**	**6.8**	**1.923**	**E3/E3**	**VI**	**NA**	**ULB LHNN**
AD 5	**110**	**F**	**60**	**24**	**3.5**	**1.91**	**E3/E3**	**V**	**4**	**ULB LHNN**
AD 6	**6365**	**M**	**57**	**19**	**3.6**	**1.921**	**E3/E4**	**VI**	**NA**	**Neuro-CEB**
AD 7	**7238**	**M**	**79**	**28**	**6.8**	**1.912**	**E3/E4**	**VI**	**4**	**Neuro-CEB**
AD 8	**4319**	**F**	**90**	**32**	**4.3**	**1.918**	**E2/E4**	**VI**	**NA**	**Neuro-CEB**
AD 9	**5389**	**F**	**79**	**24**	**5.7**	**1.924**	**E3/E4**	**VI**	**4**	**Neuro-CEB**
AD 10	**78**	**F**	**91**	**5.5**	**5.7**	**1.923**	**E3/E4**	**V**	**2**	**ULB LHNN**
AD 11	3105	M	74	10	2.6	1.886	E3/E3	VI	NA	Neuro-CEB
AD 12	5946	F	89	10	2.5	1.887	E2/E3	VI	NA	Neuro-CEB
AD 13	7853	F	86	30	2.6	1.932	E3/E3	VI	5	Neuro-CEB
AD 14	7871	M	71	6	3.1	1.919	E3/E3	VI	NA	Neuro-CEB
AD 15	5848	F	91	26	2.5	1.941	E3/E3	VI	NA	Neuro-CEB
AD 16	8629	M	81	17.5	2.8	1.932	E3/E3	VI	5	Neuro-CEB
AD 17	4278	M	67	19	2.3	1.894	E3/E4	VI	NA	Neuro-CEB
AD 18	5036	M	61	24	3.1	1.829	E3/E4	VI	3	Neuro-CEB
AD 19	6563	M	82	25	2.9	1.934	E3/E4	VI	5	Neuro-CEB
AD 20	7141	M	76	9.5	2.7	1.927	E3/E4	VI	NA	Neuro-CEB
AD 21	8105	F	80	24	2.9	1.924	E3/E4	VI	4	Neuro-CEB
AD 22	3742	F	63	28	3.2	1.896	E3/E4	VI	NA	Neuro-CEB
AD 23	5796	M	70	6	2.3	1.915	E4/E4	VI	NA	Neuro-CEB

Table 1. Demographics of all subjects (n=36). Neuro-CEB is the national network of brain bank organized by a consortium of patient's associations, France. ULB LHNN is the brain bank (BB190052) at Université Libre de Bruxelles (ULB), Belgium. 19 samples with RIN value ≥ 3.5 (marked in bold) were used for next-generation sequencing and RT-qPCR analysis. When explicitly mentioned all 36 samples were used for RT-qPCR analysis. Abbreviations: AD-Alzheimer's disease, APOE- Apolipoprotein E, CTR-Control, PMD-post-mortem delay, RIN-RNA integrity number, and NA-Not available. Temporal superior T1 isocortex region was used from brain banks. Details on comorbid neuropathological conditions: Sample IDs 8010, 7238, 7853, 8629, 7141, and 8105 had cerebral amyloid angiopathy; 6563 had cerebral amyloid angiopathy with Lewy body disease; and 5389 had cerebral amyloid angiopathy with limbic-predominant age-related TDP-43 encephalopathy. Comorbid neuropathological data for the remaining cases were unavailable.

miRNAs	Direction of observation in this study (NGS)	AD reports in Brain (Direction and Regions)	AD reports in CSF
miR-129-5p	Down	Down Temporal cortex[43],	Down[51]

ARTICLE IN PRESS

		Superior temporal gyrus and Entorhinal cortex[20], Hippocampus and Prefrontal cortex[42], Dorsolateral prefrontal cortex[47,48]	
miR-146b-5p	Down	Down Hippocampus and Medial frontal gyrus[52], Frontal cortex[53,54], Dorsolateral prefrontal cortex[47]	Down[52,55]
miR-18a-5p	Up	Up Prefrontal cortex[42], Frontal cortex[54]	_
miR-132-5p	Down	Down Superior temporal gyrus and Entorhinal cortex[20], Prefrontal cortex[42], Frontal cortex[54], Dorsolateral prefrontal cortex[47,48], Inferior frontal gyrus and Superior temporal gyrus[58], Hippocampus, Temporal gyrus and Frontal gyrus[40]	_
miR-151a-5p	Up	Up Frontal cortex[54]	Up[52]
miR-133a-3p	Down	_	_
miR-1-3p	Down	Up Inferior frontal gyrus and Superior temporal gyrus[58]	_
novel-miR-71	Down	_	_
novel-miR-122	Up	_	_
miR-151b	Up	_	Up[52]
miR-132-3p	Down	Down Hippocampus[19], Hippocampus and Prefrontal cortex[42], Frontal cortex[53,54], Dorsolateral prefrontal cortex[47,48], Inferior frontal gyrus and Superior temporal gyrus[58], Hippocampus, Temporal cortex and Frontal cortex[66], Temporal gyrus and Frontal gyrus[40], Hippocampus and Temporal cortex[76], Temporal cortex and Frontal cortex[46], Superior and mid temporal neocortex[41], Temporal cortex[77]	Down[51]
miR-3065-3p	Up	Up Frontal cortex[54]	_

ARTICLE IN PRESS

ARTICLE IN PRESS

miR-129-1-3p	Down	Down Dorsolateral prefrontal cortex[48], Frontal cortex[53], Temporal cortex[43,46]	–

Table 2. Comparison of miRNAs identified by NGS in this study with AD reports.

Figure captions

Figure 1. Differentially expressed miRNAs in the temporal superior T1 isocortex of AD patients compared to control (CTR). a) Representative digital gel showing variable RNA quality with RIN values obtained for post-mortem brain samples with the Agilent analyzer. b) Correlation plot between PMD and the RIN for all 36 post-mortem brain samples. c) Range of RIN values (minimum in red and maximum in green) in the existing reports of AD post-mortem brain studies[20,39-44]. d) Flow chart shows the scheme for enriching 13 miRNAs in selected 19 subjects (control-9 and AD-10). e) Volcano plot shows 5 upregulated (red) and 8 downregulated (blue) with criteria (p value <0.003, FDR/padj < 0.1 and |log2 fold change|>=0.45) in selected 19 subjects (control-9 and AD-10). Abbreviations: DLPFC-Dorsolateral prefrontal cortex, GM-Gray matter and WM-White matter.

Figure 2. Box plots showing normalized counts for 13 miRNAs that were differentially expressed in temporal superior T1 isocortex of AD patients compared to control (CTR). 8 miRNAs were downregulated a) miR-129-5p, b) miR-146b-5p, d) miR-132-5p, f) miR-133a-3p, g) miR-1-3p, h) novel-miR-71, k) miR-132-3p, and m) miR-129-1-3p and 5 miRNAs were upregulated c) miR-18a-5p, e) miR-151a-5p, i) novel-miR-122, j) miR-151b, and l) miR-3065-3p in AD (n=10) compared to the control (n=9) subjects. In each box plot, significance values (p and FDR) and fold change (FC) were shown. miRNAs were considered differentially expressed with the cut of p value <0.003, FDR <0.1 and|log2 fold change|>=0.45. Boxplots show the interquartile range (IQR), median and whiskers (1.5× IQR).

Figure 3. Correlation analyses of RIN, PMD, age, and miRNAs based on NGS data in 19 subjects a) Matrix showing correlation among the RIN, PMD, age, and 13 differentially expressed miRNAs. Positive correlations are displayed in blue and negative correlations in red. Size of the circle and colour intensity are proportional to the correlation coefficients. b and c) Correlation plots among the 5 high abundance miRNAs: miR-129-5p, miR-146b-5p, miR-151a-5p, miR-1-3p, miR-132-3p. d) Correlation plots for mature miRNAs with common precursor miRNA.

Figure 4. Validation of differentially expressed miRNAs by RT-qPCR in temporal superior T1 isocortex of AD patients compared to control (CTR) in 19 subjects. a) 11 miRNAs with fold change for CTR and AD. U6 was used as normalizer. b) Levels of 5 high abundance miRNAs along with miR-16-5p and miR-30b-5p (shaded in gray) in CTR and AD patients based on NGS data. c) Correlation plot between RIN and Ct values for U6, miR-16-5p and miR-30b-5p. d) Fold change for 5 high abundance miRNAs with three different normalizers U6 (shaded in blue), miR-16-5p (shaded in green) and miR-30b-5p (shaded in red). Welch Two Sample t-test was performed between the groups for each normalizer in (a) and (d). In a) and d) RNA samples were same, but different cDNA preparation and qPCR plating was performed. Boxplots show the interquartile range (IQR), median and whiskers (1.5× IQR).

Figure 5. miRNA expression across the Braak stages in 19 subjects. Normalized counts of NGS data are plotted along the Braak stages for a) miR-129-5p b) miR-146b-5p c) miR-151a-5p d) miR-1-3p and e) miR-132-3p. Fold change of RT-qPCR are plotted along the Braak stages for f) miR-129-5p g) miR-146b-5p h) miR-151a-5p i) miR-1-3p and j) miR-132-3p. U6 was used as normalizer. One-way ANOVA test was

ARTICLE IN PRESS

ARTICLE IN PRESS

performed and ANOVA p value was mentioned in black and post–hoc Tukey HSD test p value (only significant) was mentioned in gray in (a) to (j). Boxplots show the interquartile range (IQR), median and whiskers (1.5× IQR).

Figure 6. miRNA association with tau pathology based on Braak stages and tau phosphorylation (PHF1) in 19 subjects. a) Western blot probed for PHF1 in RIPA-soluble fraction of CTR (n=9) and AD (n=10) post-mortem T1 isocortex. b) Matrix showing correlation among the NFT (Braak stages), PHF1 (OD), and miRNAs (based on NGS data). Positive correlations are displayed in blue and negative correlations in red. Size of the circle and colour intensity are proportional to the correlation coefficients. c) Correlation between the Braak stages and densitometric analysis of PHF1 (OD) signal. d) Correlation between the 5 high abundance miRNAs with the Braak stages. e) Correlation between the 5 high abundance miRNAs with the densitometric analysis of PHF1 (OD) signal. Controls are shaded in light orange in (c-e). Abbreviation: OD-Optical density.

Figure 7. miRNAs modulate tau seeding in HEK biosensor cells. a) Procedure to obtain sarkosyl-insoluble fraction. b) Electron microscopy negative staining confirms the presence of PHFs in AD sarkosyl-insoluble fraction. Scale bar-50 nm. c) Western blot analyses showing PHF-tau species in the AD sarkosyl-insoluble fraction but not in the control fraction using PHF1 and total tau antibodies. d) FACS analyses show no FRET signal for CTR sarkosyl-insoluble fraction but striking FRET signal for AD sarkosyl-insoluble fraction treated biosensor cells. e) Heatmap shows relative FRET signals of mimic and inhibitors with AD sarkosyl-insoluble fraction that are normalized to only AD sarkosyl-insoluble fraction treated biosensor cells (n=3). f) Quantification of FRET signals from FACS for miR-146b-5p and miR-151a-5p (n=3). g) FRET signals illustrated by microscopy. Scale bar-50 µm. One-way ANOVA with post–hoc Tukey HSD test was performed in (f). Boxplots show the interquartile range (IQR), median and whiskers (1.5× IQR).

Figure 8. miRNA target and pathway enrichment analysis. a) Shows the KEGG pathways enriched for targets predicted for downregulated and upregulated miRNAs in AD. b) miRNA-target network for downregulated miRNAs in AD. Blue represents miRNA, and an increase in the size of the blue circle denotes more predicted targets for the miRNA. Pink represents target mRNA, and a larger colored circle indicates a highlighted target mRNA in the six selected pathways. Yellow represents target mRNA in Neurotrophin signaling pathway, gray represents target mRNA in Dopaminergic, Serotonergic, and Cholinergic synapses, green represents target mRNA in Axon guidance, cyan represents target mRNA in Long-term depression, and red represents target mRNA in Alzheimer's disease.

ARTICLE IN PRESS

ARTICLE IN PRESS

Editor Summary

Profiling of microRNAs reveals their dysregulation in the Alzheimer's disease brain. Further biochemical analysis shows their association with tau pathology and a potential role in modulating the progression of tau pathology.

Peer Review Information

Communications Biology thanks Long Wang, Alyssa Walker and the other, anonymous, reviewer(s) for their contribution to the peer review of this work. Primary Handling Editors: Rosie Bunton-Stasyshyn & Joao de Sousa Valente. A peer review file is available.

ARTICLE IN PRESS

ARTICLE IN PRESS

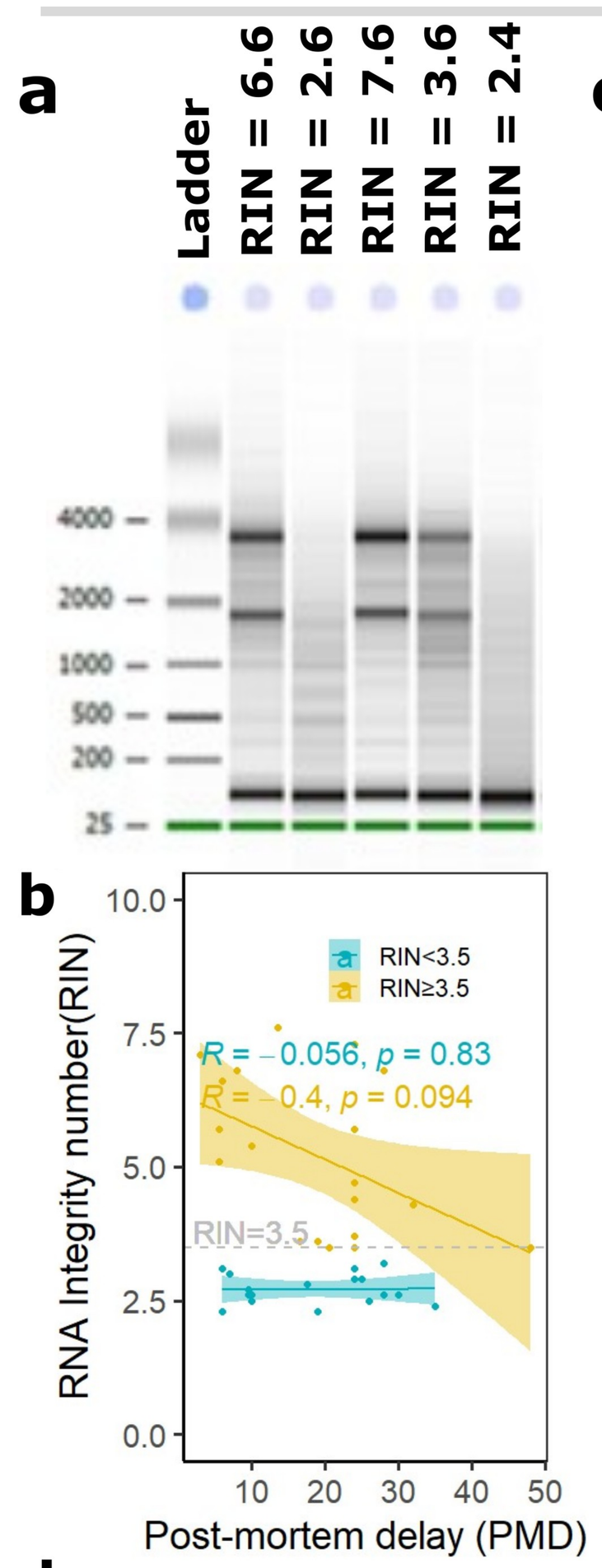

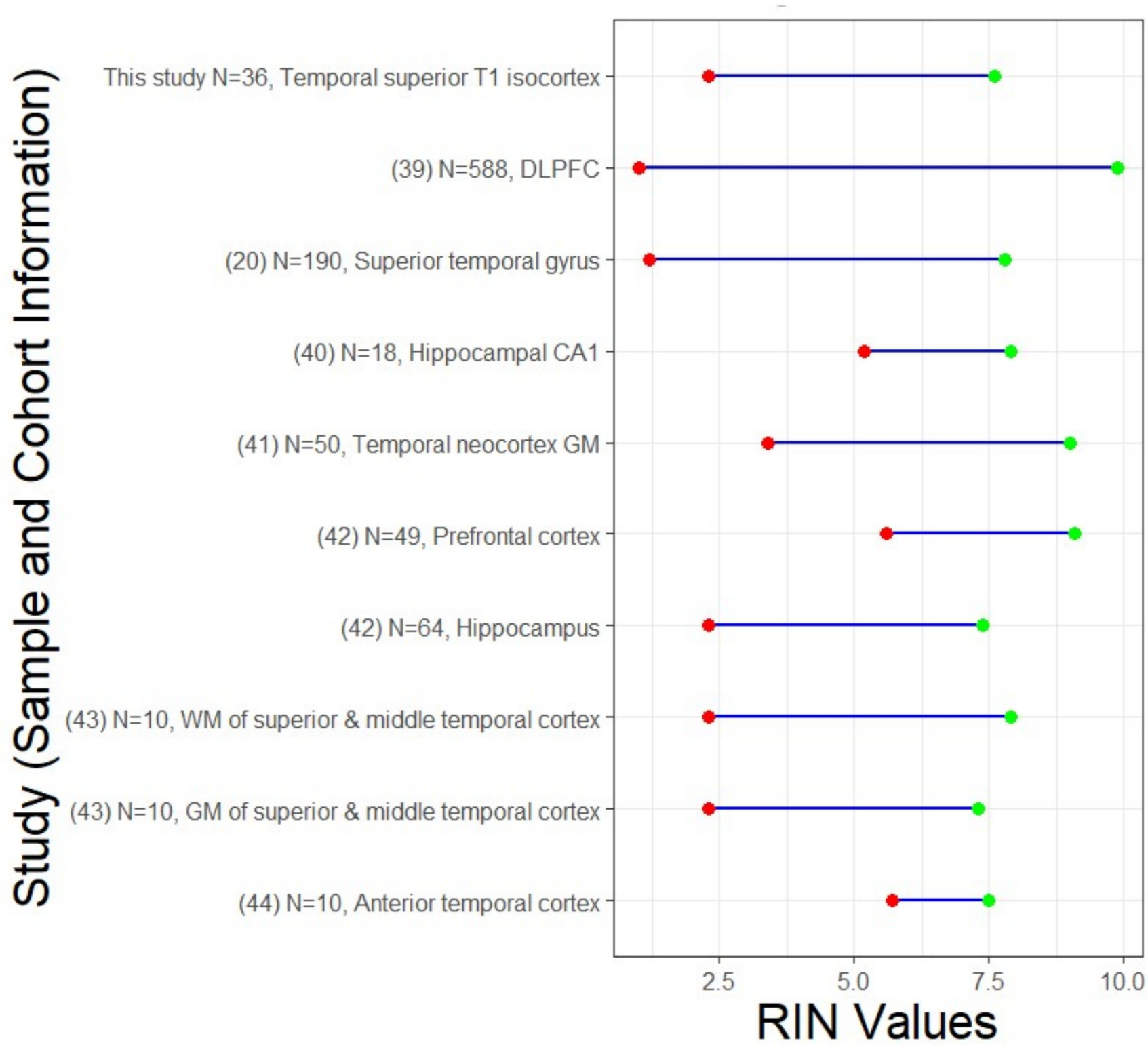

d

CTR-9 and AD-10

Total = 19

449 miRNA counts

⬇

57 Differentially expressed miRNAs (p value < 0.05)

⬇

13 Differentially expressed miRNAs (p value < 0.003 and padj < 0.1)

5 upregulated

8 downregulated

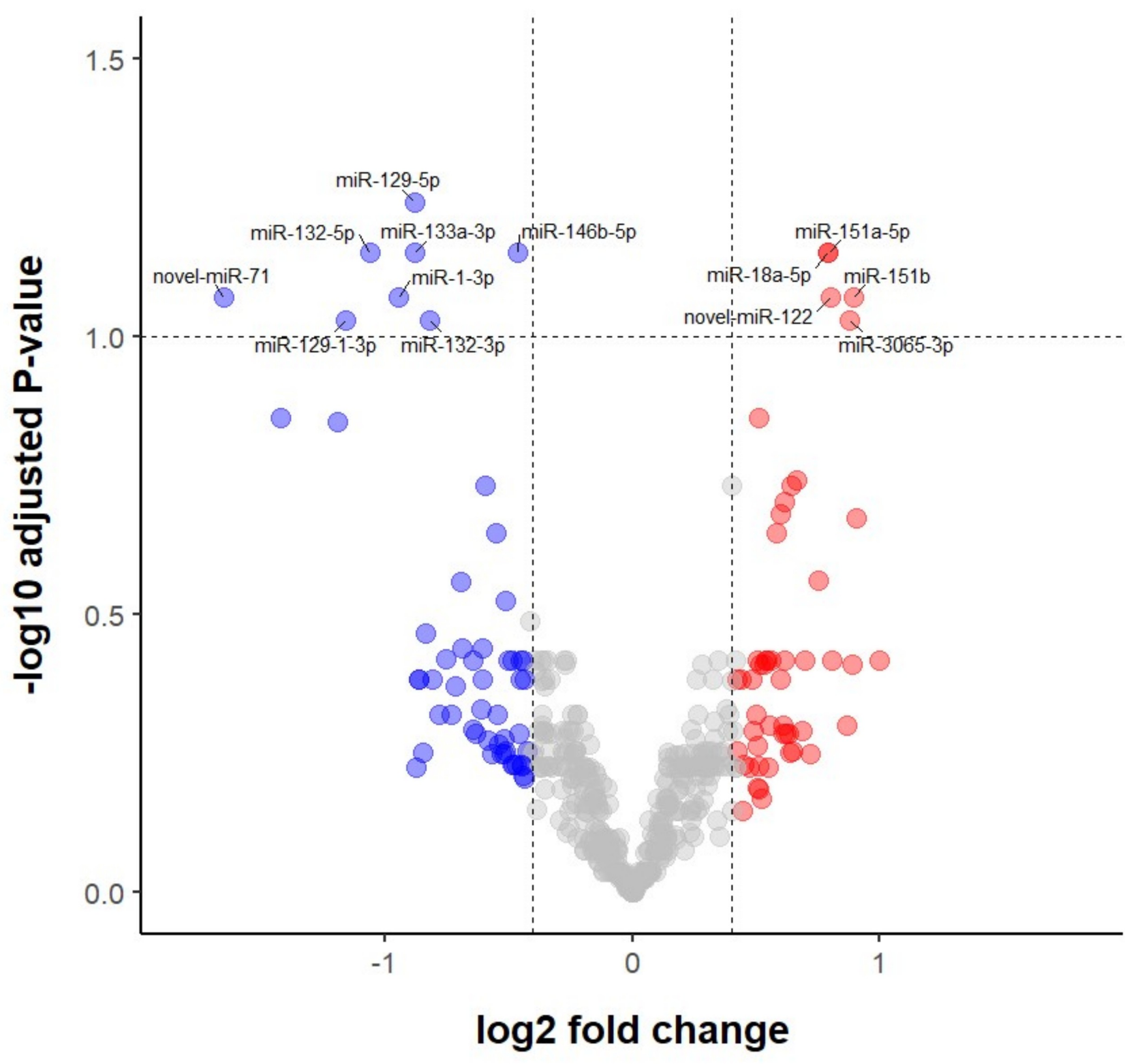

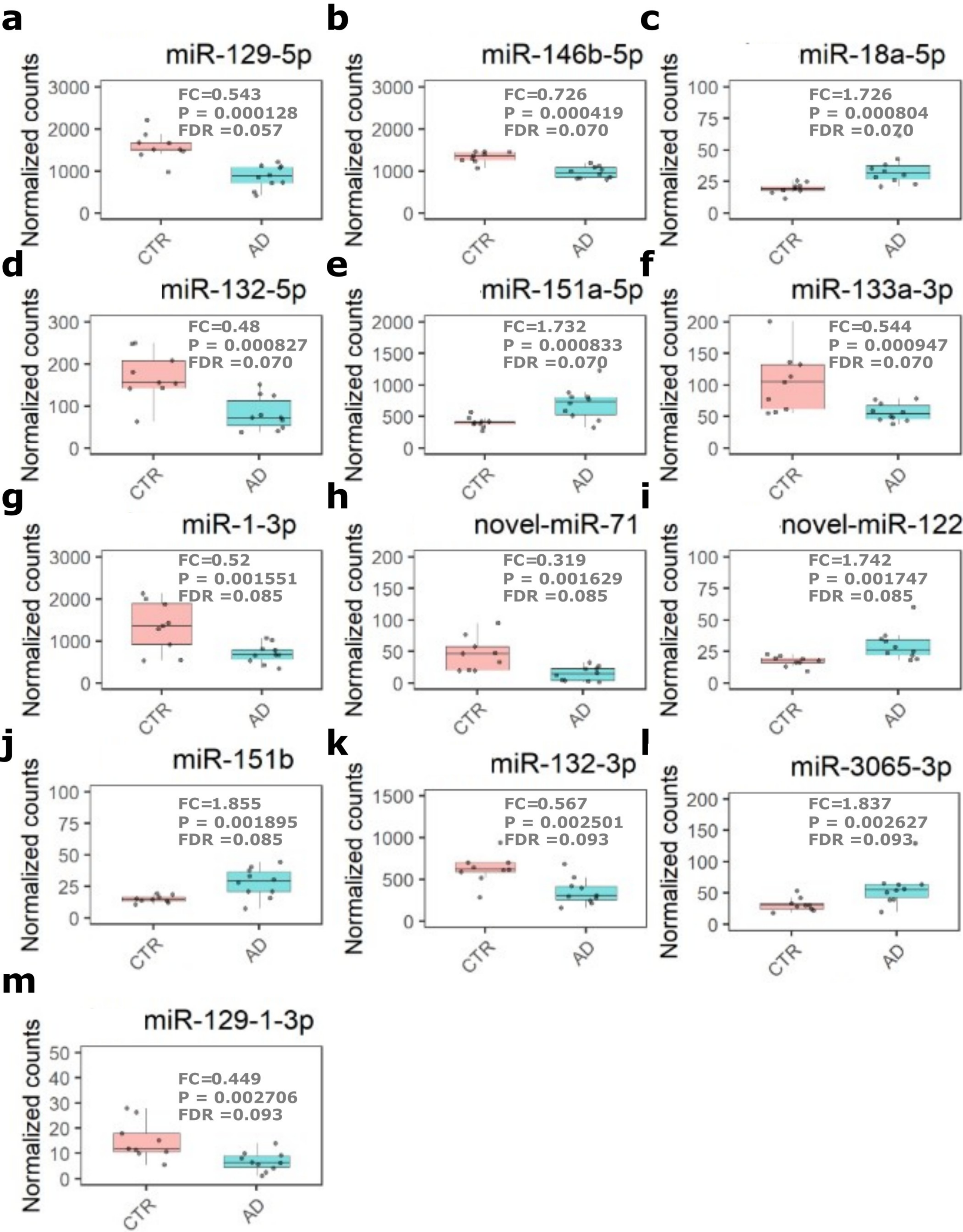
a
miR-129-5p
FC=0.543
P = 0.000128
FDR =0.057
b
miR-146b-5p
FC=0.726
P = 0.000419
FDR =0.070
c
miR-18a-5p
FC=1.726
P = 0.000804
FDR =0.070
d
miR-132-5p
FC=0.48
P = 0.000827
FDR =0.070
e
miR-151a-5p
FC=1.732
P = 0.000833
FDR =0.070
f
miR-133a-3p
FC=0.544
P = 0.000947
FDR =0.070
g
miR-1-3p
FC=0.52
P = 0.001551
FDR =0.085
h
novel-miR-71
FC=0.319
P = 0.001629
FDR =0.085
i
novel-miR-122
FC=1.742
P = 0.001747
FDR =0.085
j
miR-151b
FC=1.855
P = 0.001895
FDR =0.085
k
miR-132-3p
FC=0.567
P = 0.002501
FDR =0.093
l
miR-3065-3p
FC=1.837
P = 0.002627
FDR =0.093
m
miR-129-1-3p
FC=0.449
P = 0.002706
FDR =0.093
Normalized counts
CTR
AD

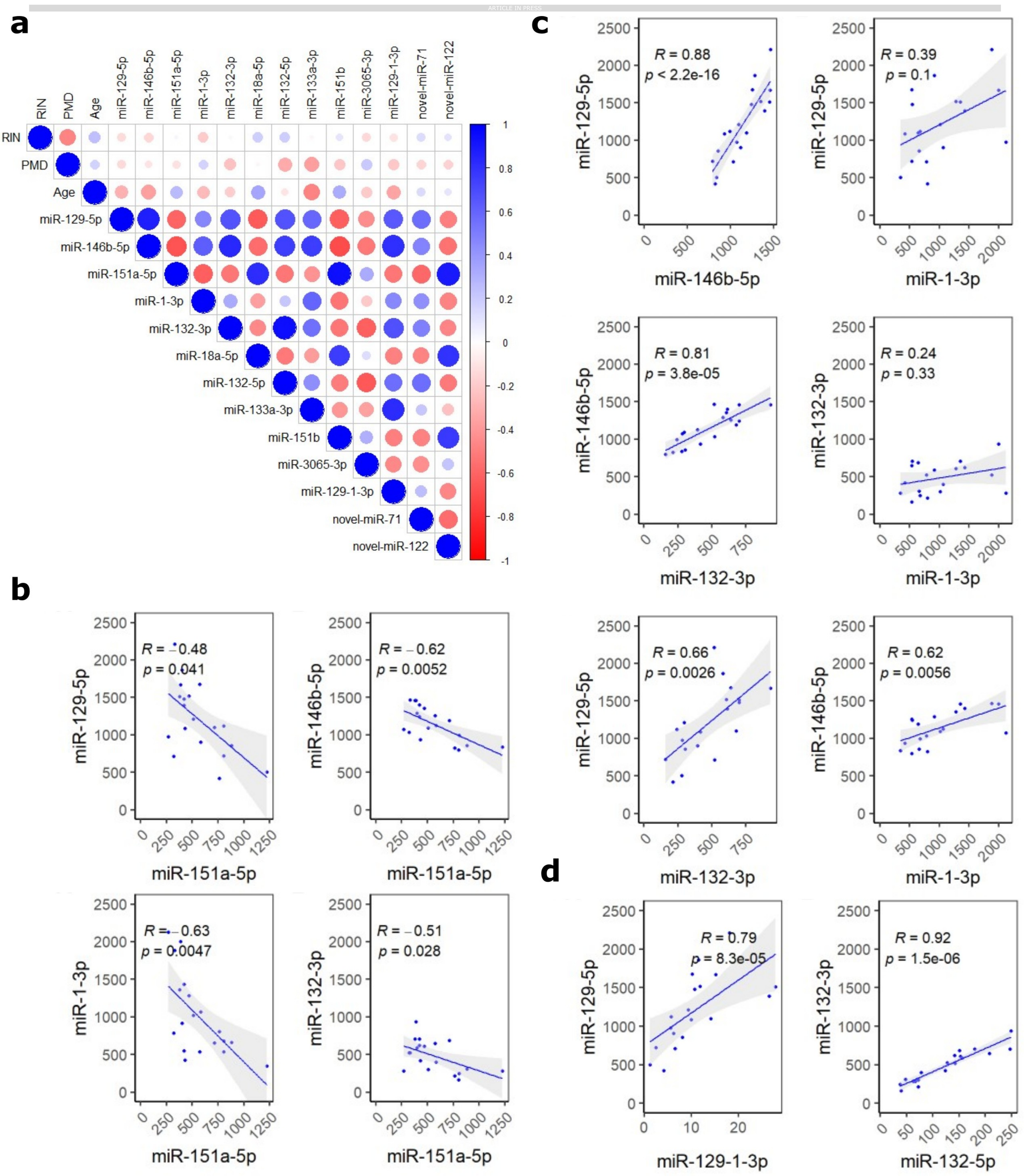
a
RIN
PMD
Age
miR-129-5p
miR-146b-5p
miR-151a-5p
miR-1-3p
miR-132-3p
miR-18a-5p
miR-132-5p
miR-133a-3p
miR-151b
miR-3065-3p
miR-129-1-3p
novel-miR-71
novel-miR-122
1
0.8
0.6
0.4
0.2
0
-0.2
-0.4
-0.6
-0.8
-1
c
R = 0.88
p < 2.2e-16
miR-129-5p
miR-146b-5p
R = 0.39
p = 0.1
miR-129-5p
miR-1-3p
R = 0.81
p = 3.8e-05
miR-146b-5p
miR-132-3p
R = 0.24
p = 0.33
miR-132-3p
miR-1-3p
b
R = −0.48
p = 0.041
miR-129-5p
miR-151a-5p
R = −0.62
p = 0.0052
miR-146b-5p
miR-151a-5p
R = 0.66
p = 0.0026
miR-129-5p
miR-132-3p
R = 0.62
p = 0.0056
miR-146b-5p
miR-1-3p
R = −0.63
p = 0.0047
miR-1-3p
miR-151a-5p
R = −0.51
p = 0.028
miR-132-3p
miR-151a-5p
d
R = 0.79
p = 8.3e-05
miR-129-5p
miR-129-1-3p
R = 0.92
p = 1.5e-06
miR-132-3p
miR-132-5p

ARTICLE IN PRESS

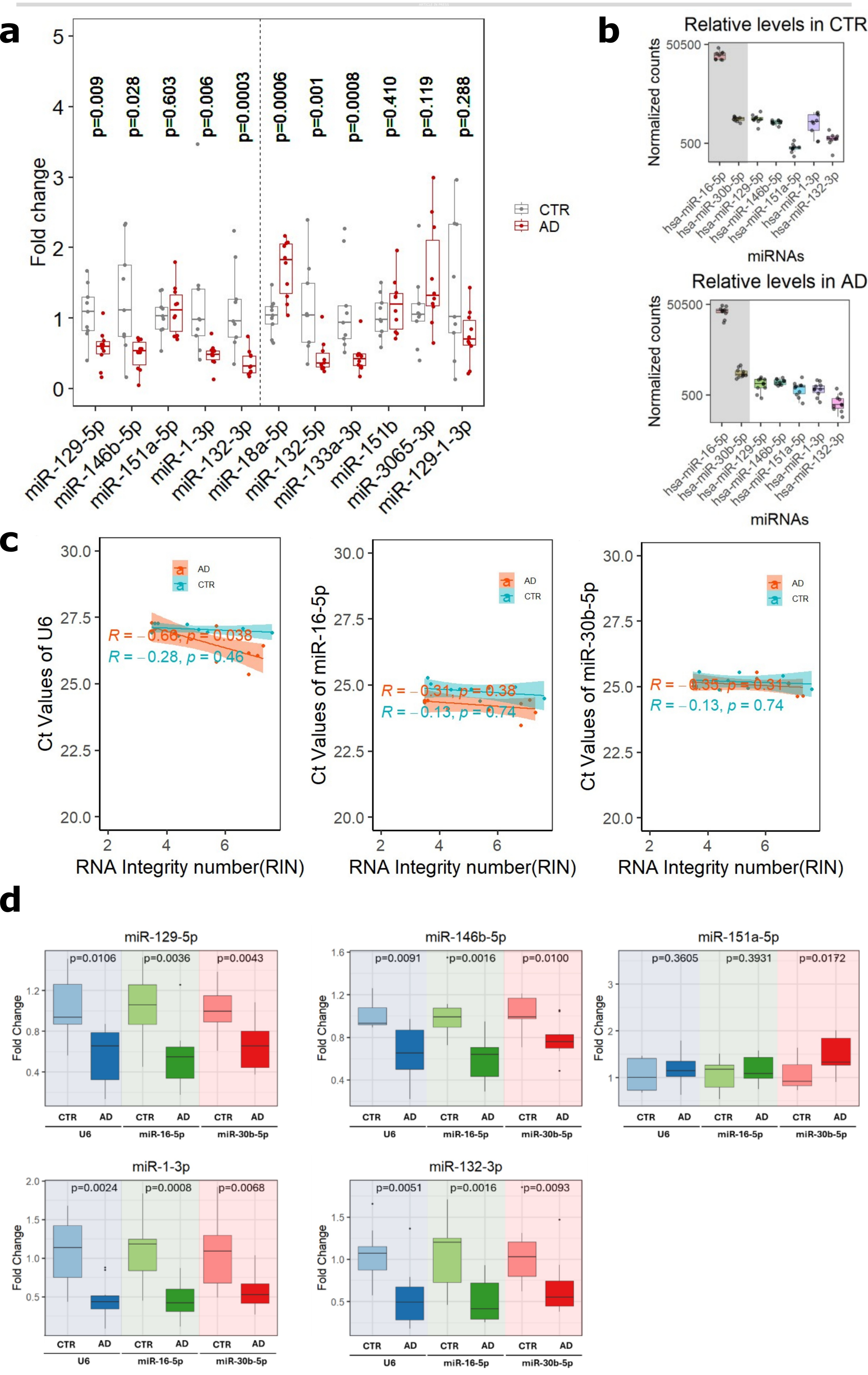

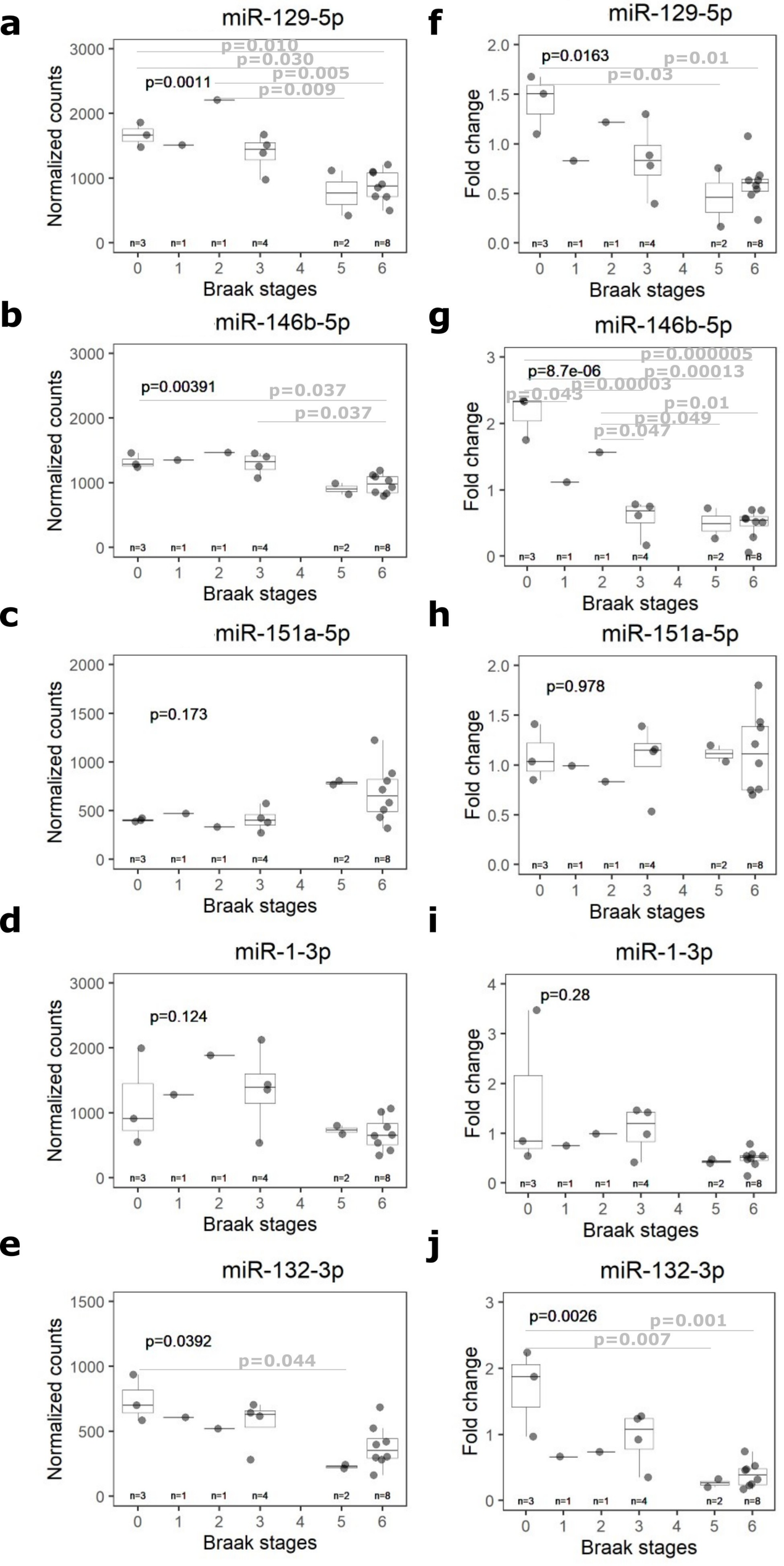
a
miR-129-5p
Normalized counts
p=0.0011
p=0.010
p=0.030
p=0.005
p=0.009
n=3 n=1 n=1 n=4 n=2 n=8
Braak stages
b
miR-146b-5p
Normalized counts
p=0.00391
p=0.037
p=0.037
Braak stages
c
miR-151a-5p
Normalized counts
p=0.173
Braak stages
d
miR-1-3p
Normalized counts
p=0.124
Braak stages
e
miR-132-3p
Normalized counts
p=0.0392
p=0.044
Braak stages
f
miR-129-5p
Fold change
p=0.0163
p=0.01
p=0.03
Braak stages
g
miR-146b-5p
Fold change
p=8.7e-06
p=0.000005
p=0.00013
p=0.00003
p=0.043
p=0.01
p=0.049
p=0.047
Braak stages
h
miR-151a-5p
Fold change
p=0.978
Braak stages
i
miR-1-3p
Fold change
p=0.28
Braak stages
j
miR-132-3p
Fold change
p=0.0026
p=0.001
p=0.007
Braak stages

ARTICLE IN PRESS

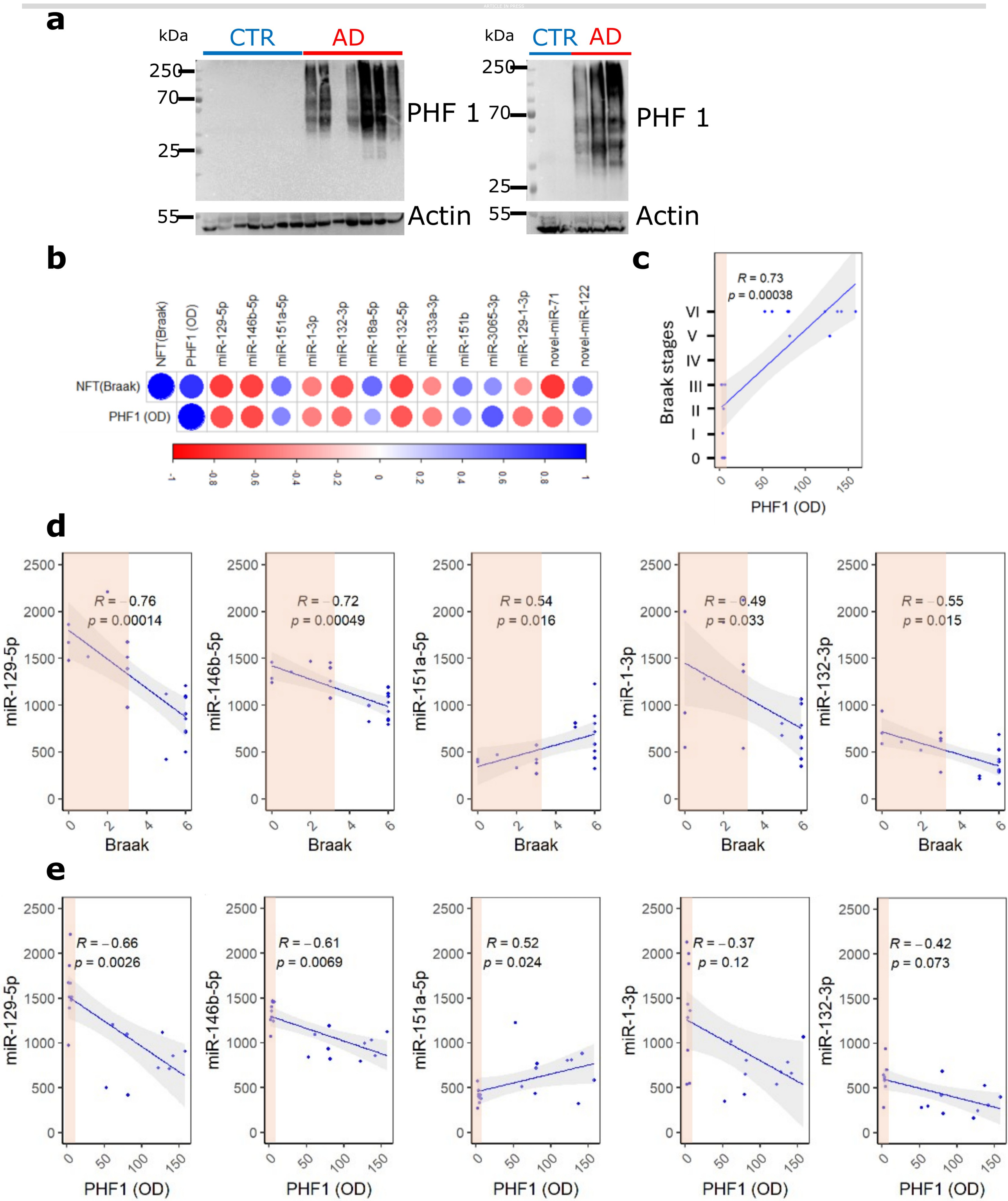

ARTICLE IN PRESS

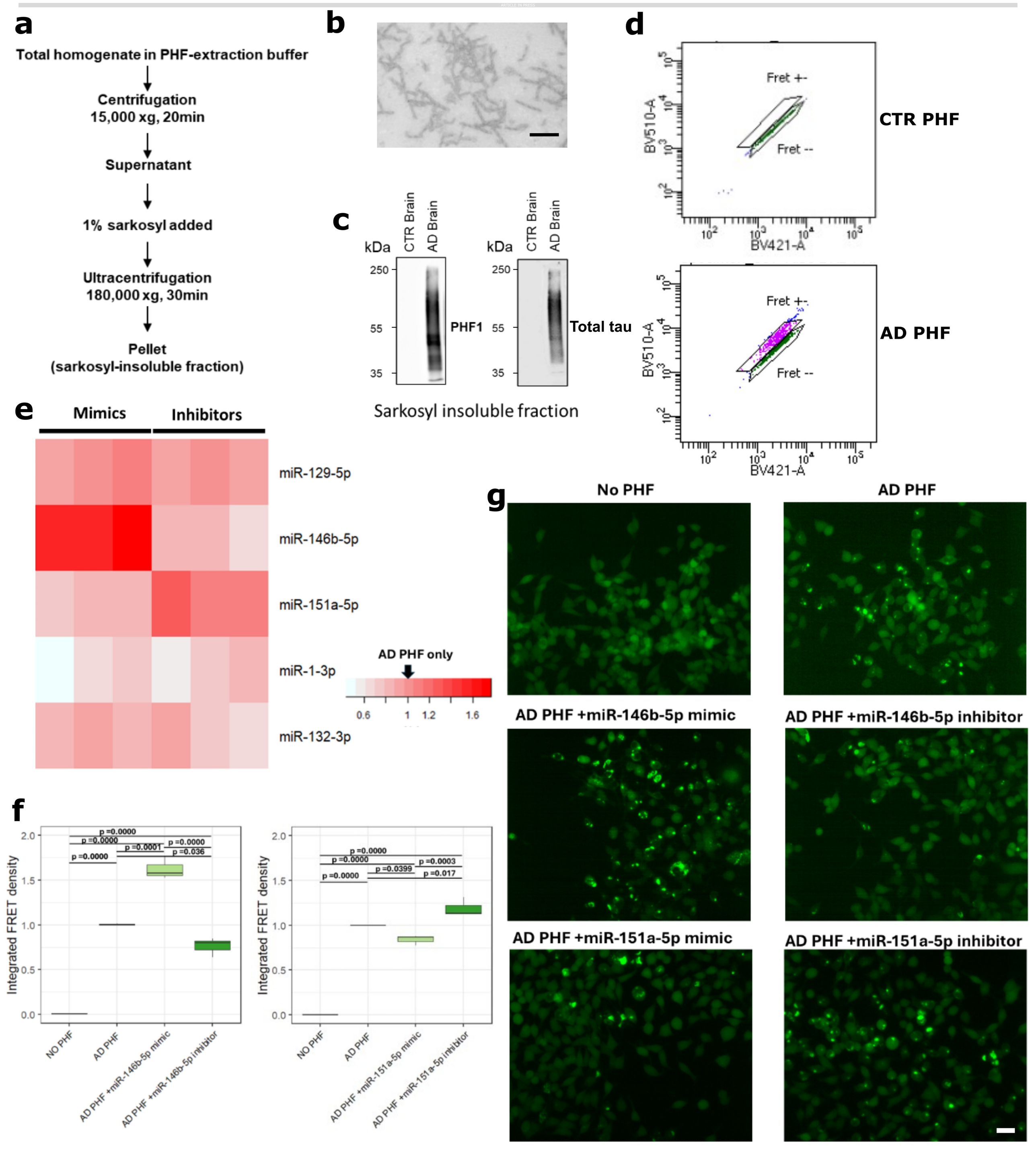

a

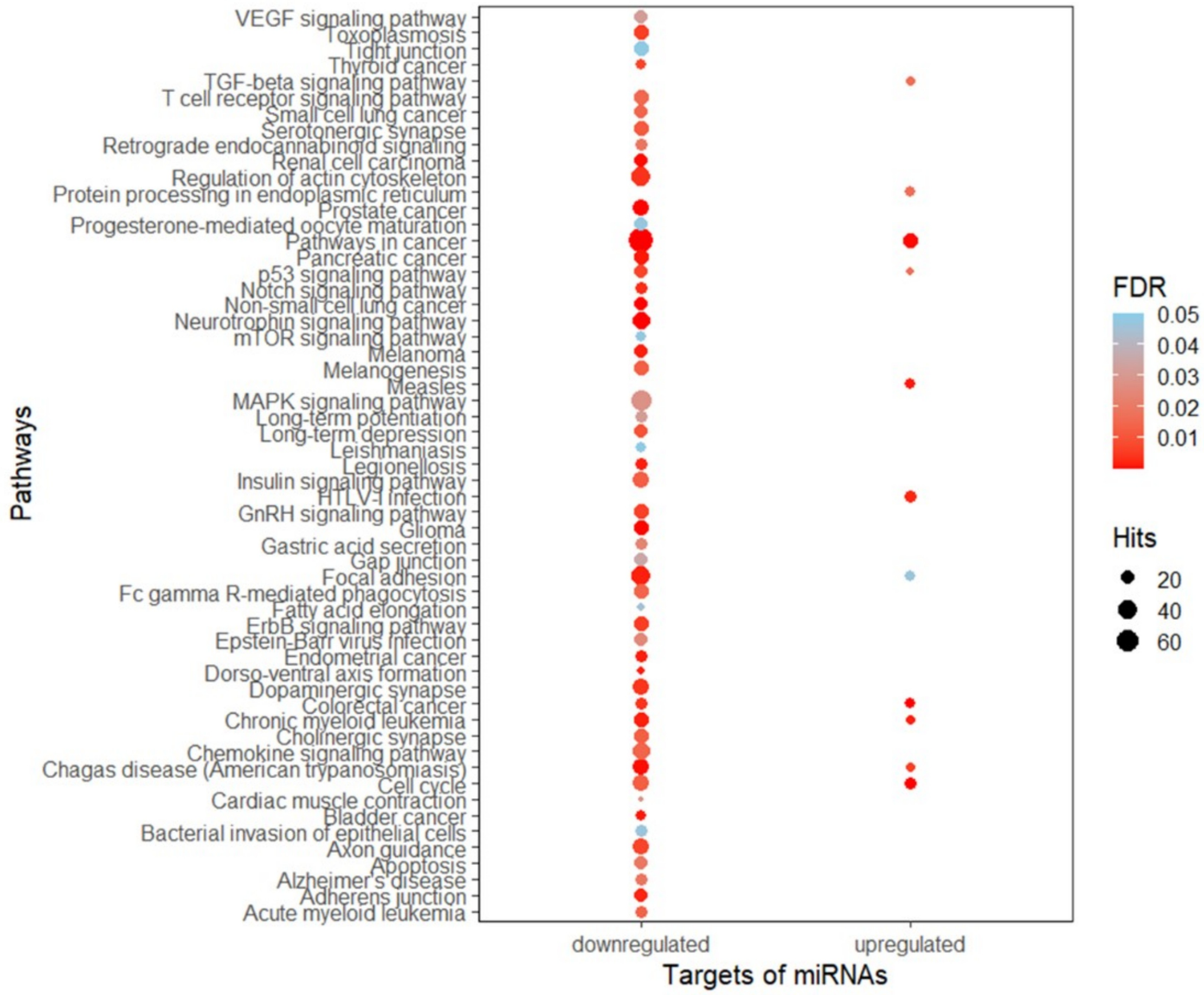
VEGF signaling pathway
Toxoplasmosis
Tight junction
Thyroid cancer
TGF-beta signaling pathway
T cell receptor signaling pathway
Small cell lung cancer
Serotonergic synapse
Retrograde endocannabinoid signaling
Renal cell carcinoma
Regulation of actin cytoskeleton
Protein processing in endoplasmic reticulum
Prostate cancer
Progesterone-mediated oocyte maturation
Pathways in cancer
Pancreatic cancer
p53 signaling pathway
Notch signaling pathway
Non-small cell lung cancer
Neurotrophin signaling pathway
mTOR signaling pathway
Melanoma
Melanogenesis
Measles
MAPK signaling pathway
Long-term potentiation
Long-term depression
Leishmaniasis
Legionellosis
Insulin signaling pathway
HTLV-I infection
GnRH signaling pathway
Glioma
Gastric acid secretion
Gap junction
Focal adhesion
Fc gamma R-mediated phagocytosis
Fatty acid elongation
ErbB signaling pathway
Epstein-Barr virus infection
Endometrial cancer
Dorso-ventral axis formation
Dopaminergic synapse
Colorectal cancer
Chronic myeloid leukemia
Cholinergic synapse
Chemokine signaling pathway
Chagas disease (American trypanosomiasis)
Cell cycle
Cardiac muscle contraction
Bladder cancer
Bacterial invasion of epithelial cells
Axon guidance
Apoptosis
Alzheimer's disease
Adherens junction
Acute myeloid leukemia
Pathways
downregulated
upregulated
Targets of miRNAs
FDR
0.05
0.04
0.03
0.02
0.01
Hits
20
40
60

b

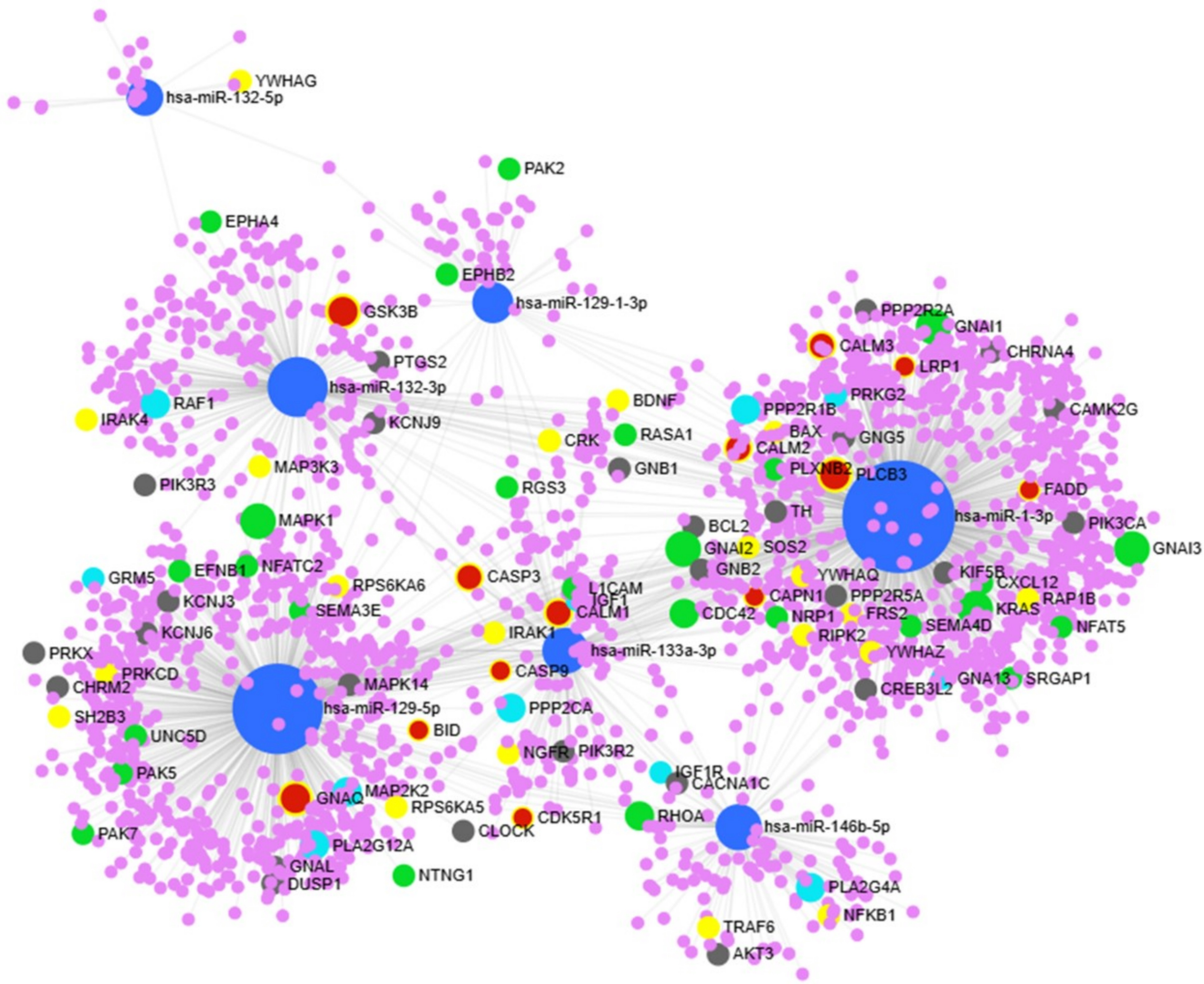
YWHAG
hsa-miR-132-5p
PAK2
EPHA4
EPHB2
hsa-miR-129-1-3p
GSK3B
PTGS2
hsa-miR-132-3p
RAF1
IRAK4
KCNJ9
MAP3K3
PIK3R3
MAPK1
EFNB1
NFATC2
GRM5
KCNJ3
RPS6KA6
SEMA3E
KCNJ6
PRKX
PRKCD
CHRM2
SH2B3
UNC5D
PAK5
PAK7
MAPK14
hsa-miR-129-5p
BID
GNAQ
MAP2K2
RPS6KA5
PLA2G12A
GNAL
DUSP1
NTNG1
BDNF
CRK
RASA1
GNB1
RGS3
CASP3
L1CAM
IGF1
CALM1
IRAK1
hsa-miR-133a-3p
CASP9
PPP2CA
NGFR
PIK3R2
CDK5R1
CLOCK
PPP2R2A
GNAI1
CALM3
CHRNA4
LRP1
PRKG2
PPP2R1B
CAMK2G
BAX
GNG5
CALM2
PLXNB2
PLCB3
FADD
TH
hsa-miR-1-3p
PIK3CA
BCL2
GNAI2
SOS2
GNAI3
GNB2
YWHAQ
KIF5B
CXCL12
CAPN1
PPP2R5A
RAP1B
CDC42
NRP1
FRS2
KRAS
SEMA4D
NFAT5
RIPK2
YWHAZ
GNA13
SRGAP1
CREB3L2
IGF1R
CACNA1C
RHOA
hsa-miR-146b-5p
PLA2G4A
NFKB1
TRAF6
AKT3